Ocean Modelling 129 (2018) 39–57

Contents lists available at ScienceDirect

Ocean Modelling

journal homepage: www.elsevier.com/locate/ocemod

Waves along Eastern boundary currents – The regional winds effect

Alvaro Semedo[a,*], Pedro M.M. Soares[b], Gil Lemos[b]

[a] IHE Delft, Department of Water Science and Engineering, Westvest 7, 2611 Delft, the Netherlands
[b] Instituto Dom Luiz (IDL), Faculdade de Ciências, Universidade de Lisboa, 1749-016 Lisboa, Portugal

ABSTRACT

The wind fields along the five eastern boundary currents (EBC) systems (California, Canary, Humboldt, Benguela, and West Australia) are highly seasonal. This seasonality is mostly determined by the position of the semi-permanent high pressure cells over the ocean. During summer these high pressure cells, with a thermal low pressure systems inland, are the synoptic drivers of along coast winds. These strong summer winds, along the EBC systems, off-shore mid-latitude continental coasts, generate waves that can be rather extreme, considering that these areas can be seen as limited fetch wave fields. A qualitative analysis of the wave climate over the mid-latitudes western coastal areas, along the five EBC systems, based on the ERA-Interim reanalysis wave data, is presented. The influence of coastal wind speed intensification processes in these areas, like the occurrence of coastal low-level jets, and expansion fans in the lee of headlands and capes, on the local wave field is studied. It is shown that, despite the distance between the five EBC systems, their wave fields, particularly during summer, are very similar when the wind sea and swell characteristics are balanced. In summer locally generated wave heights and energy content, along EBC areas, are comparable or even higher than swell ones.

1. Introduction

Wind-waves are the inevitable consequence of the wind action over the air-sea interface, with gravity acting as the restoring force (hence they can also be called "surface gravity waves"). Wind-waves (henceforth simply called waves) mediate the exchange of primarily momentum between winds and the ocean surface. But they also modulate exchanges of heat, mass, and gases between the ocean and the atmosphere, also altering the radiative characteristics of the ocean surface (Babanin et al., 2012). Waves therefore play an important role in the coupled ocean-atmosphere climate system (Rutgersson et al., 2010; Cavaleri et al., 2012; Patricola et al., 2016). While generated by the local wind, waves have the ubiquitous characteristic of propagating away from their generating area. For that reason, at the ocean surface, two types of waves coexist. Waves under growing process, intimately coupled with the local wind field, are called wind sea. Once these waves propagate away from their generation area, out-speeding the local wind and no longer receiving energy from it, they are called swell. Swells can travel across entire ocean basins, losing very little energy (Ursel, 1956; Munk et al., 1963; Snodgrass et al., 1966; Young et al., 1999; Alves, 2006, Ardhuin et al., 2009) before they eventually shoal and break at a coast. Swell waves can be called as young or old swells, depending on the distance to their generation area. It is because swells can propagate long distances that the wave field in the open ocean is most of the times the result of contributions from local and remotely generated waves, with different origins and ages (Hanley et al., 2010; Semedo et al., 2008; Semedo, 2010). Recently, it has been shown that swell dominates the global wave field (Chen et al., 2002; Semedo et al., 2011) even along the main wave generation areas, along the northern and southern hemisphere extratropical storm paths.

Several observational studies (e.g. Drennan et al., 1999, Smedman et al., 1999, 2009, Hogstrom et al., 2009, 2013) have shown that waves impact on the air-sea exchanges is sea state dependent, *i.e.*, it depends on the qualitative characteristics of the wave field, being influenced by the prevalence of one type of waves over the other. When swell waves propagate into light wind areas, with phase speeds much higher than the local wind speed, they can have an impact on the lower atmosphere, inducing a pressure perturbation in the first few meters of the marine atmospheric boundary layer (MABL). In these situations, waves lose energy to the atmosphere as they propagate (Ardhuin and Jenkins, 2006), and accelerate the airflow at lower altitudes in the form of the so called "wave driven wind" (Harris, 1966; Sullivan et al., 2008) or "wave driven low level-jet" (Hogstrom et al., 2009). This acceleration of the flow at low levels induces a departure from the logarithmic wind profile (Semedo et al., 2009, Nilsen et al., 2012). For this reason, swell has a consistent influence in the overall structure of the MABL in light wind areas, since it reduces the wind shear in the boundary layer and consequently the mechanical production of turbulence (Smedman et al., 1999; Potter, 2015). On the other hand, under the wave generating process, momentum is transferred from the atmosphere into the ocean. This momentum is extracted from the wind field (Jansen et al., 2002; Janssen, 2004), generating waves, but also driving

* Corresponding author.
E-mail address: a.semedo@un-ihe.org (A. Semedo).

https://doi.org/10.1016/j.ocemod.2018.07.005
Received 25 October 2017; Received in revised form 12 May 2018; Accepted 17 July 2018
Available online 19 July 2018

wind currents and triggering wave breaking and whitecapping (Koeman et al., 1994, 1998). Waves also induce the so called wave induced currents at the ocean surface (Stokes, 1847), that are mostly driven by wind sea waves (McWilliams and Restrepo, 1999; Carrasco et al., 2014). The wave breaking and white-capping that occurs in high wind speed regimes, when waves are being generated, enhances the turbulence in the ocean surface mixing layer, with great influence in the mass and gas transfer between the ocean and the lower atmosphere (Semedo et al., 2009; Babanin, 2011). While the influence of swell waves in the MABL can extend up to the top of the boundary layer (Sullivan et al., 2008), in wind sea dominated areas, when waves are being generated, the effect of waves is restricted to the first few meters of the atmosphere (Janssen, 2004; Hristov et al., 2003).

The climatological global wave heights resemble the global surface marine wind field. The mean near-surface wind speeds and the correspondent extremes are highest in the mid- to high-latitudes, along the extratropical storm tracks, with seasonal climatological maxima in the hemisphere winter (Gulev et al., 2003, Caires and Sterl, 2005; Young, 1999; Semedo et al., 2011; Stopa et al., 2014). Wind speeds are lowest in the tropical and low latitudes. Nevertheless, although some connection exists, the climatological global significant wave heights (SWH) do not exactly match the overlaying local marine wind field, due to the propagating effect of waves. This detachment between winds and wave heights ends up being highest in the inter-tropical latitudes. There the mean surface wind speeds are low, but north and south bound swell waves, generated in the mid-latitudes, prevail (Young, 1999), having almost no relation with the local wind field (Semedo, 2010).

Hanley et al. (2010) and Semedo et al. (2011) showed that in most areas of the world ocean the wave field is dominated by swell, more than 75% of the time, even along the intense wind speed extratropical storm tracks. In some areas the wave field characteristics have a strong seasonality, for example in marginal or enclosed seas (Cavaleri et al., 1991; Tuomi et al., 2011; Galanis et al., 2012; Semedo et al., 2014). This is also the case along equator-ward eastern boundary currents (EBC) systems, as already noticed by Semedo et al. (2011), where coast parallel strong local winds can occur, playing an important role in the definition of regional wave climates. These winds in the eastern flanks of the semi-permanent subtropical high-pressure cells, along the five EBC systems, are highly seasonal. The semi-permanent high pressure highs are part of the poleward branch of the Hadley cells, with a pronounced intra-annual seasonality. In winter, due to the equatorward migration of the semi-permanent highs, the winds in the west mid-latitude coastal areas are mostly from the west and northwest (Ranjha et al., 2013; Lima et al., 2018). During summer the high-pressure systems migrate poleward and are more prevalent, and thermal low pressure systems develop inland towards the east, due to the day-time radiative heating increase. Persistent equatorward coastal parallel wind features develop as the geostrophically adjusted response to the correspondent synoptic pattern: a high-pressure over the ocean and a low pressure inland (Rijo et al., 2015; Lima et al., 2018). These winds are strongly linked to regional ocean dynamics, with impacts both in the atmosphere and the ocean, through an intrinsic atmosphere-ocean coupling process (Beardsley et al., 1987). They drive upwelling along the mid-latitude west coasts, due to offshore Ekman transport, bringing cold water to the surface (Vallis, 2012, Rijo et al., 2017). The low sea surface temperature (SST) along the mid-latitude continental west coasts in summer, further sharpens the temperature and pressure gradients, driving a local wind speed increase right at the coast. It is within these coast parallel strong winds that, mostly in summer, coastal low-level jets (CLLJ; Winant et al., 1988, Ranjha et al., 2013) develop. That is the case off the coasts of: California-Oregon, along the California Current, Iberia and Northwest Africa, along the Canary Current, Chile, along the Humboldt Current, Namibia-Angola, along the Benguela Current, and West Australia, along the West Australian Current. The previously mentioned synoptic and regional patterns, responsible for these coastal winds, start to build during late spring and lasts until early fall (Ranjha et al., 2013; Soares et al., 2014; Rijo et al., 2014, 2017; Lima et al., 2018). Although the interaction between the winds and the upwelling along EBC systems has been relatively well documented in previous studies (e.g. Bakun, 1990, Gersbach et al., 1999, Small and Nicholls, 2003; Mohtadi et al., 2005, Narayan et al., 2010; Miranda et al., 2013), that is not the case of the regional wave climate in these areas. Due to the strong seasonality of these coast parallel regional winds, the wave climate characteristics there is also highly seasonal. A qualitative analysis of the wave climate over the mid-latitudes western coastal areas, along the five EBC systems, is precisely the main goal of this study.

The need for a qualitative analysis of the sea state characteristics has two fundamental reasons. On the one hand, as mentioned above, the air-sea interaction and exchanges are sea state dependent, hence the need to understand which type of waves are more prevalent in a specific area. On the other hand, characterizing the wave climate in a specific area (or globally), by using the traditional SWH and mean wave period (MWP) parameters, might not be enough, since they provide a limited description of the sea-state. Two wave fields with the same SWH and MWP may still be different in detail, because they can be more or less dominated by one type of waves (Holthuijsen, 2007, Semedo et al., 2011). The SWH and MWP are integrated parameters, computed directly from the wave spectra. Different sea states, for example, resulting from a light to moderate wind condition with incoming propagating swell, and a locally generated wind sea from local winds can have similar SWH, or even MWP. For this reason a more detailed investigation is needed to correctly characterize the wave field characteristics and the wave climate of a certain ocean area. That is the case of the mid-latitudes eastern continental coastal areas along the EBC systems, where the wind regime varies considerably from winter to summer (Ranjha et al., 2013; Lima et al., 2018), potentially inducing similar variations on the regional wave fields.

Wind sea and swell wave parameters can be investigated separately by the partitioning of the wave spectra into a high and low frequency parts (Gerling, 1992; Hanson and Phillips, 2001). The availability of wave spectra observations is scarce, even in coastal areas. Wave spectra observation are available from in situ buoy measurements, mostly in coastal areas in the northern hemisphere. These point observations are nevertheless sparse, and frequently have continuity problems due to gaps in the wave records, and are therefore not suited for wave climate studies in large areas. Coastal HF (high frequency) radars can also provide wave spectra observations, but the coverage is also limited and do not offer long enough data sets. Remote sensing synthetic aperture radar (SAR) could be an alternative to wave buoys, since they provide collocated wind and wave spectra observations. Nevertheless, the retrieval of wave spectra from SAR observations still poses problems that limit its use for wave climate purposes (Pandian et al., 2011), particularly due to the fact that the high frequency part of the wave spectra is most of the times not observed (Kuo et al., 1998, Violante-Carvalho et al., 2005). Wave models are a good alternative to the limitations imposed by in situ and remote sensing observations, offering global wave spectral data with the adequate temporal and spatial resolution. Wave reanalyses, despite some problems, like the lack of homogeneity (Sterl, 2004; Stopa and Cheung, 2014) or even some shortcomings related to long term tendencies (Aarnes et al., 2015) are, so far, the only global wave dataset that can be used for wave climate qualitative studies, where wave spectra are needed.

Here a detailed study of the wave climate along EBC systems is presented, following the previous studies of Semedo et al. (2011, 2014), and the studies of Raza et al. (2013) and Lima et al. (2018) where the coastal winds in these areas where analyzed. Ranjha et al. (2013) identified 6 major areas of occurrence of coastal low-level jets: along EBC systems and along the coast of Oman (see also Ranjha et al., 2015a). Our study is restricted to the five main upwelling areas of the ocean, along the EBC systems. The current study uses the European Centre for Medium-Range Weather Forecasts (ECMWF) ERA-Interim reanalysis (Dee et al., 2011). The regional distribution and seasonal variation of the wind sea and swell SWH and MWP parameters, and how they combine in the total SWH and MWP, are presented. The analysis of the prevalence of one type of waves over the other, from an energy and predominance point of view, is also examined.

The remainder of the paper is organized as follows. The ERA-Interim reanalysis and the details about how wind sea and swell parameters are computed are presented in Section 2. Section 3 presents the climatology of the regional wind sea and swell characteristics in each of the five EBC systems, and these results are discussed in Section 4. The paper ends with the concluding remarks in Section 5.

2. Data and methodology

2.1. ERA-Interim reanalysis data

Reanalyses have the goal of overcoming inhomogeneities related to model and data assimilation upgrades that occur regularly in operational forecasting models. Unfortunately, inhomogeneities due to uneven data coverage in time and changes in observation systems remain (Uppala, 1997; Sterl, 2004; Aarnes et al., 2015; Stopa et al., 2016). In the present study wind and wave data from the ECMWF ERA-Interim reanalysis are used. ERA-Interim is a third-generation reanalysis of meteorological observations, starting in 1979, and being updated almost in real time. The ERA-Interim was produced using the ECMWF Integrated Forecasting System (IFS; release cycle Cy31r2): a two-way coupled atmosphere-wave model system (Janseen et al., 2002; Janssen, 2004), and it includes both atmospheric and wave variables. It is in fact the only reanalysis (along with ERA-40; Uppala et al., 2005) that outputs wave parameters, and assimilates wave data through a 4DVAR (four-dimensional variational) data assimilation scheme (Dee et al., 2011, Lorenc and Rawlins, 2005). Observations of ocean wind speeds from VOS (voluntary observing ships), buoys, and remote sensing satellite scatterometery have been assimilated in the reanalysis process. Satellite altimetry wave heights were also assimilated since 1991. The wave model used in the IFS coupled model system was the third-generation WAM model (WAMDI Group, 1988; Komen et al., 1994). The horizontal resolution of the atmospheric model is approximately 79 km (T255 spectral truncation) on a reduced Gaussian grid, while the wave model is run with shallow water physics, with a horizontal resolution of 1° (about 110 km). The output resolution of ERA-Interim is 6 h. The wave model set up in the ERA-Interim reanalysis uses the 2-minute gridded elevations/bathymetry data for the world (ETOPO2; NGDC 2006). Additional details about the ERA-Interim reanalysis can be found in Dee and Uppala (2009), Dee et al. (2011), and Aarnes et al. (2015). Here we use the period from 1979 to 2013.

2.2. Wave and wind parameters

Besides the total wave parameters, wind sea and swell parameters are also used in the present study, with the goal of assessing, qualitatively, the role of local and remotely generated waves along EBC systems. In the wave model WAM the integrated wave parameters are computed from the two-dimensional (2D) wave energy spectra [$F(f, \theta)$, where f is the frequency and θ the propagating direction]. The wave spectra are outputted at each grid point upon solving the so called spectral wave action balance equation (WAMDI Group, 1994; Koeman et al., 1994). In the present study, the SWH, MWP and mean wave direction (MWD) parameters from the total (H_s,T_m,θ_m), swell (H_s^s, T_m^s, θ_m^s), and wind sea (H_s^w, T_m^w, θ_m^w) wave fields, respectively, are used. Besides wave parameters, wind speed (U_{10}) and the wind direction (φ) at 10 m height are also used, since the wind is a crucial parameter in the definition of the areas of study. The wind sea and the swell parameters are computed by integrating $F(f, \theta)$ over the high and low frequency parts of the energy wave spectra, respectively, separated by a characteristic frequency $\hat{f}$, corresponding to a wave phase speed:

$$\hat{c} = g(2\pi\hat{f})^{-1} = 1.2*28 \times u_{*}cos(\Delta), \tag{1}$$

where u_* is the friction velocity, and Δ is the difference between the wave propagating direction and the wind direction ($\Delta = \theta - \varphi$; Bidlot 2001). The factor 28 corresponds to the peak wave phase speed from the Pierson-Moskowitz spectrum (Pierson and Moskowitz, 1964; Alves et al., 2003), and 1.2 is a tuning parameter.

To assess the wind sea and swell wave climates along the EBC areas, the ERA-Interim wind and wave parameters were processed for seasonal statistics. Following the WMO (World Meteorological Society) standards, where seasons are defined and named as: DJF (December to February), MAM (March to May), JJA (June to August), and SON (September to November). The climatological analysis is based on the DJF and JJA seasons (winter or summer, depending on the hemisphere), despite some remarks in the text concerning MAM and SON. The analysis is focused on the mid-latitudes western coastal areas, along the five EBC: California, Canary, Humboldt, Benguela, and West Australia.

3. Waves climate along Eastern boundary currents

3.1. Global wind and wave climates

The JJA and DJF seasonal maps for the climatological mean U_{10} and φ global fields are shown in Fig. 1. As can be seen, during boreal (Fig. 1a) and austral (Fig. 1b) summers, coast parallel intense mean wind speeds occur off the mid-latitude western continental coasts, along the EBC systems. These areas of interest, where the present study will be focused, are highlighted in red boxes, in the respective hemisphere summer in Fig. 1a,b. These boxes are similar to the ones shown in Ranjha et al. (2013) and Semedo et al. (2015), where coastal jets were investigated. An exception is the area along the Canary EBC, here a single area of study is assumed here, instead of separating it into two areas: Iberia and Northwest Africa.

In JJA (Fig. 1a), the highest climatological mean wind speeds in the North Pacific sub-basin occur along the California current. These seasonal regional winds, in JJA, are in fact stronger than the larger scale winds along the North Pacific extratropical storm tracks and North Pacific Trades. To some extend a similar situation takes place during JJA in the North Atlantic sub-basin, along the Canary current, although only off the coast of Northwest Africa are the wind speeds higher than along the mid-latitude storm tracks and Trade winds paths. In DJF (Fig. 1b) the close to surface wind speed fields, in these two northern hemisphere areas, are substantially different from JJA. During boreal winter the mean wind speed is now lower there, and considerably lower than in the extratropical storm tracks and along the respective Trade Winds path.

In DJF, in the southern hemisphere, high climatological mean wind speeds also occur along the Humboldt, Benguela, and West Australia currents, off the coasts of Chile, Namibia-Angola, and West Australia, respectively. Nevertheless, in the southern hemisphere the strongest summer mean wind speeds still occur in the extratropical storm tracks, in the Southern Ocean storm belt, which displays a lower inter-seasonal variability, compared to the northern hemisphere. During the Austral winter, in these areas, the wind speed is also considerably different, with a decrease in the local wind strength and an equatorward migration of the southern hemisphere storm belt. From here onwards, when the South Pacific, Indian, and Atlantic Oceans are mentioned, it is assumed that the respective Southern Ocean sectors at higher latitudes are included, unless otherwise mentioned.

The DJF and JJA global mean SWH wave fields, generated by the close to surface winds, are shown in Figs. 2 and 3, respectively. The climatological mean H_s, H_s^s, and H_s^w, and the correspondent θ_m, θ_m^s, and θ_m^w, are shown separately, allowing the propagating effect of swell and

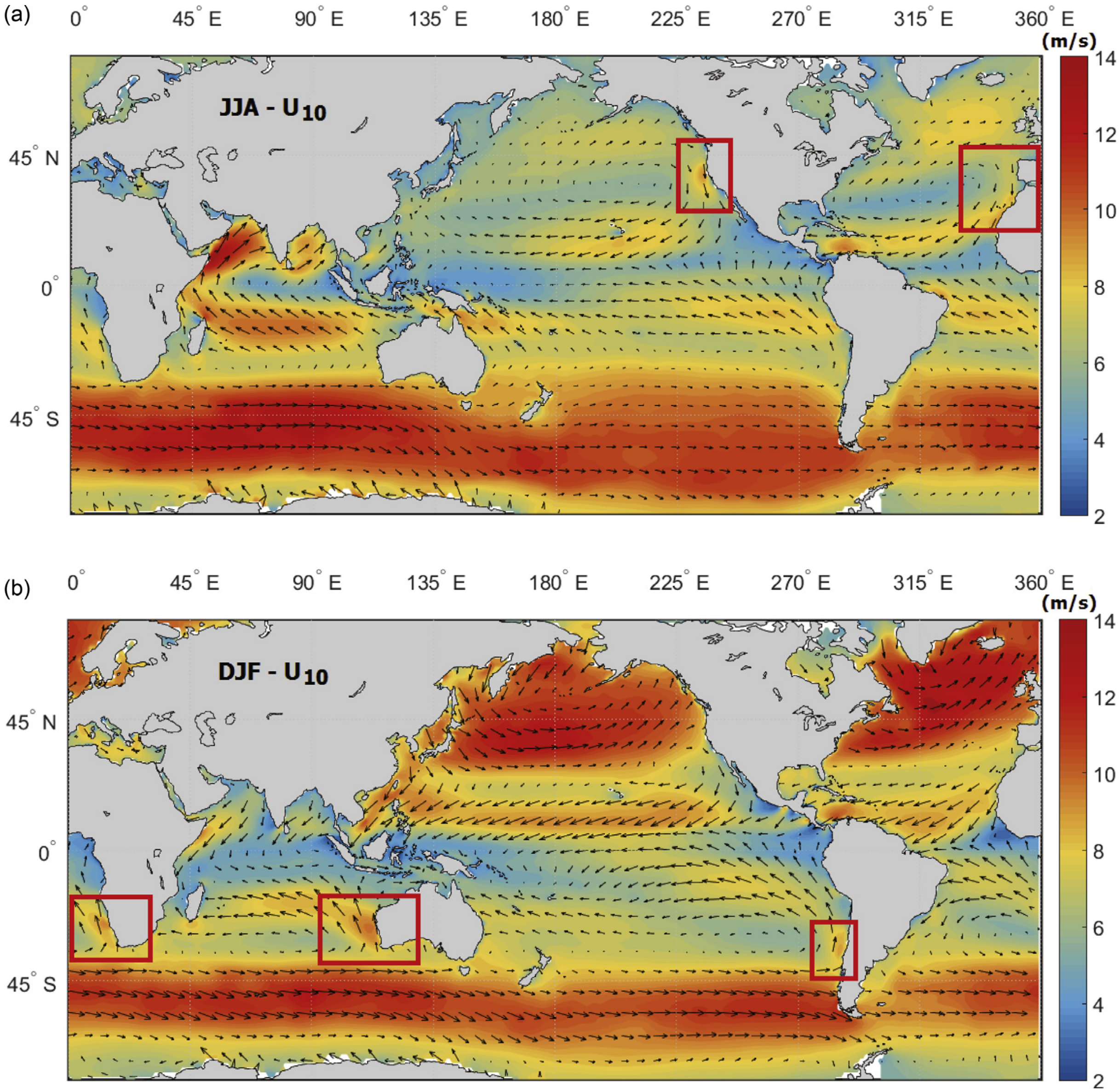

Fig. 1. Seasonal means of U_{10} (m/s) and φ (arrows; °) for (a) JJA, and (b) DJF. The arrows are scaled with the U_{10} background fields. The regions of interest are enclosed in red; (a) California and Canary currents, and (b) Humbolt (Chile), Benguela (Namibia-Angola) and West Australia.

the local generation of wind sea waves to be seen and analyzed separately and in greater detail. The seasonal large-scale mean H_s, H_s^s, and H_s^w, from ERA-40 (Uppala et al., 2005), were also presented by Semedo et al. (2008, 2011). The ERA-40 reanalysis has been shown to underforecast high and extreme wave heights (Sterl and Caires, 2005, Stopa et al., 2013). Although the comparison between ERA-40 and ERA-Interim SWH is out of the scope of this study, it is worth noticing that the climatological mean SWH are, as expected, higher in ERA-Interim, compared to the former. This is most noticeable in the mean H_s fields, along the extratropical storm tracks, in the respective hemisphere winter (with differences in excess of 0.5 m), as well as in the mean H_s^w fields, also along the storm tracks, in winter, but also along the EBC systems and the Trade Winds paths, in summer. These differences between the two most recent ECMWF reanalyses are also present in the climatological mean U_{10} fields shown in Fig. 1.

Besides the large-scale features of the global mean H_s fields (Figs. 2a and 3a), with higher seasonal mean maxima along the extratropical storm tracks during the respective hemisphere winter, particularly in the Southern Ocean (Indian sector), and larger (lower) inter-seasonal variability in the North Pacific and North Atlantic (Southern Ocean), a careful attention should be taken to the mean JJA and DJF H_s^s, and H_s^w fields. The swell propagation features away from the wave generation areas in the mid- and high latitudes towards the low latitudes are very clear (Figs. 2b and 3b), and are more noticeable than in the mean H_s fields. The swell propagation is clearer in the southern hemisphere winter (JJA), particularly in the Pacific Ocean, reaching far into the northern hemisphere, but also in the Indian Ocean, and, to a less extend, in the South Atlantic sub-basin. The highest mean H_s^w values (Figs. 2c and 3c) are found during the respective hemisphere winter, along the storm tracks. In JJA, in the North Pacific and North Atlantic the highest mean H_s^w values coincide with the high mean U_{10} values along the California and Canary EBC areas, in the North Pacific and North Atlantic, respectively (Fig. 1a). In DJF, in the southern hemisphere, the mean H_s^w values, along the Humboldt, Benguela, and Western Australia EBC areas, are not the highest in the respective sub-basins, since the climatological H_s^w maxima, despite being summer, lay

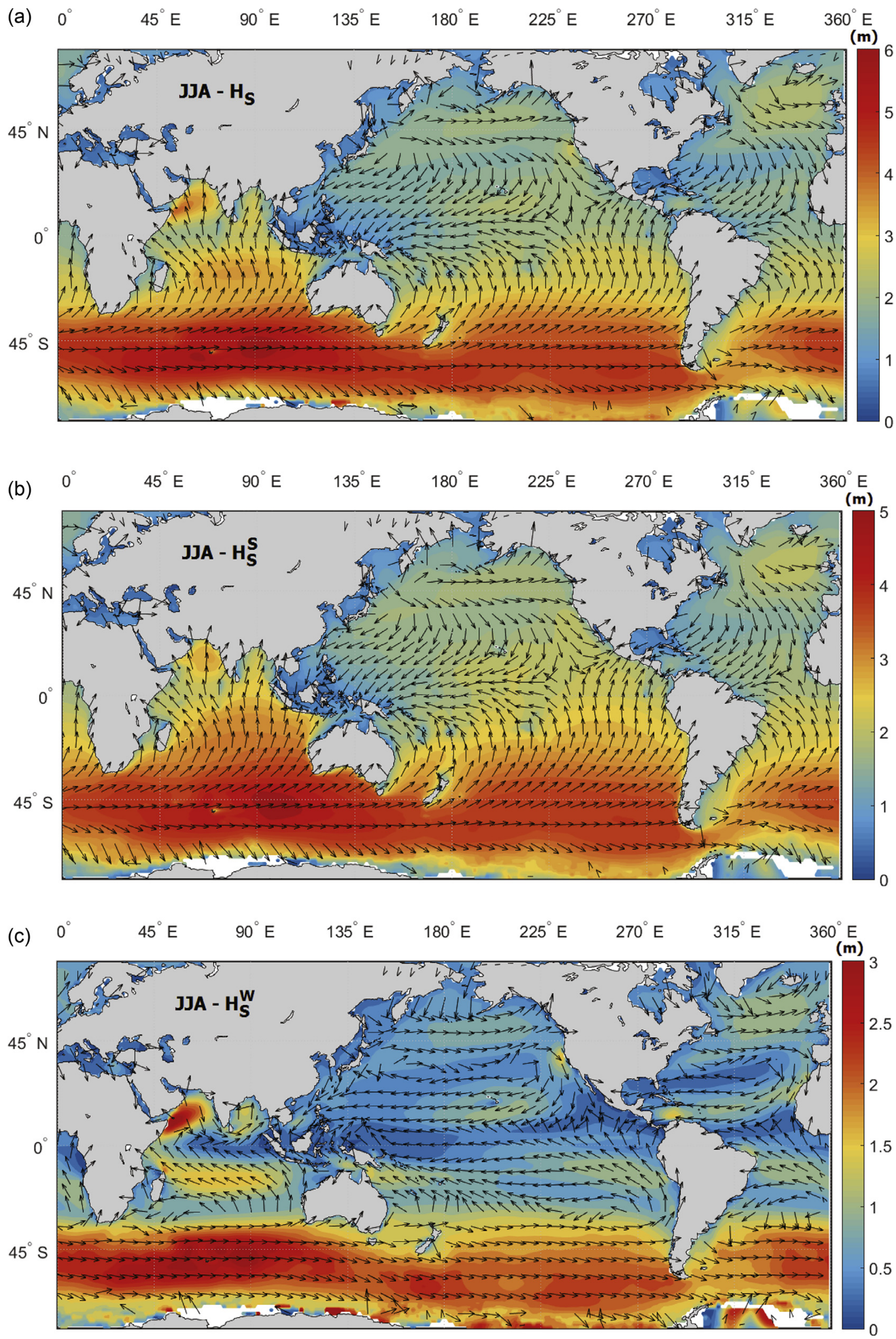

Fig. 2. Seasonal means for JJA of (a) H_s (m) and θ_m (°), (b) H_s^s (m) and θ_m^s (°), and (c) H_s^w (m) and θ_m^w (°). The arrows are scaled with the background fields. The color scales vary between the panels.

along the intense extratropical storm tracks in the Southern Ocean, as for the mean U_{10} values (Fig. 1b). The lowest mean H_s^w values are found in the low latitudes, regardless of the season (also in MAM and SON; not shown). The general features of the mean H_s^w and U_{10} are very similar (which does not happen between H_s^s and U_{10}), reflecting the coupling between both fields. This similarity is particularly noticeable along the five areas of study, in the respective summer, when U_{10} increases, as does the local H_s^w. The alignment between θ_m^w and φ along the EBC areas (coast parallel) is also noticeable.

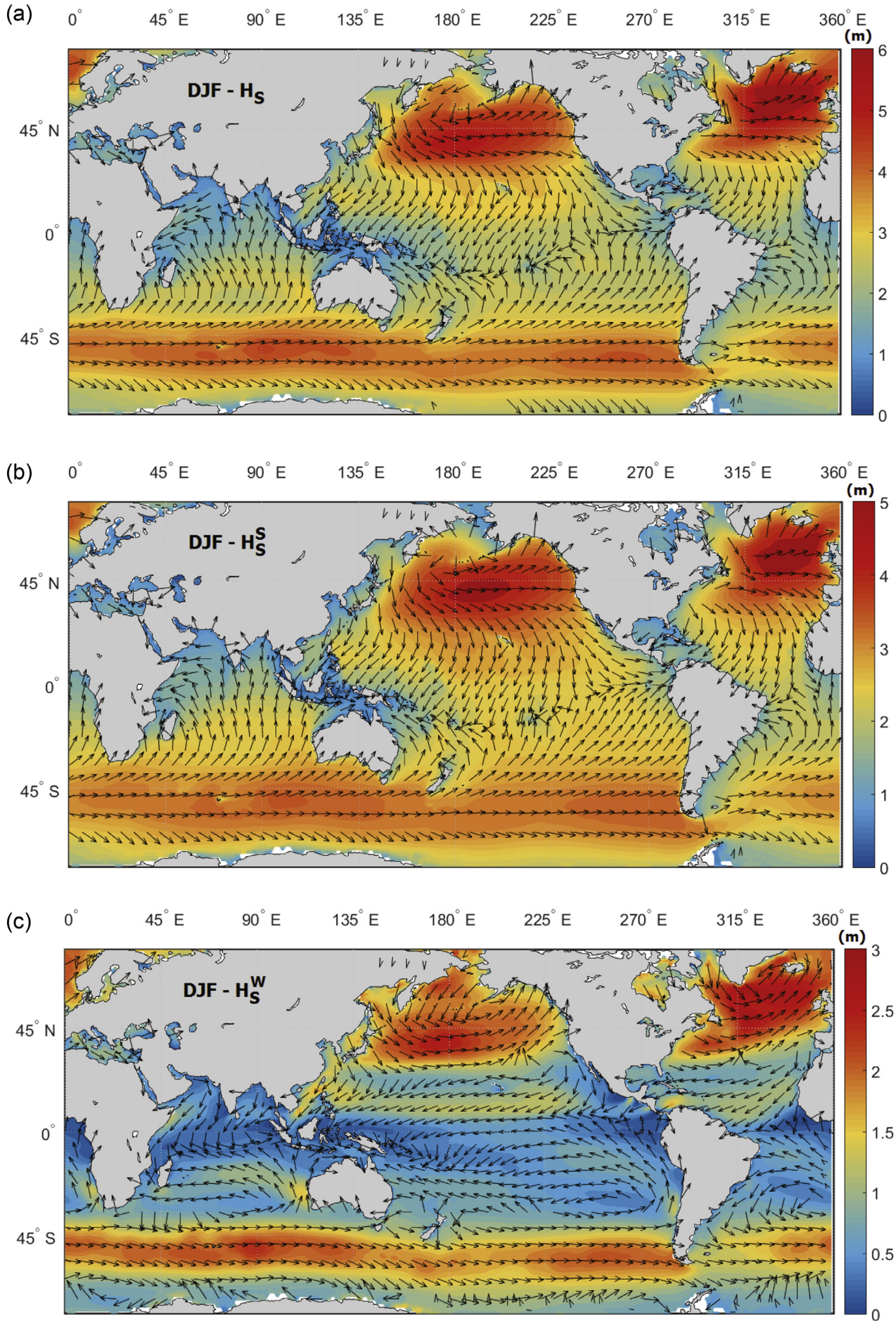

Fig. 3. Same as in Fig. 2 but for DJF. The color scales vary between the panels.

3.2. Regional wave climates

A detailed analysis of the wave climate along the five EBC systems is presented in Figs. 4–8. The mean and extreme values of wind sea and swell parameters are shown, allowing a comparison between the wave climates along the five areas of interest. The summer (JJA or DJF, depending on the hemisphere) climatological spatial distribution of the mean H_s^w 99% percentile, as well as the ratios between H_s^s and H_s^w, P_w^s and P_w^w (where P_w^s and P_w^w are the swell and wind sea wave energy fluxes, respectively), H_s^s and H_s^w 99% percentiles, P_w^s and P_w^w 99%

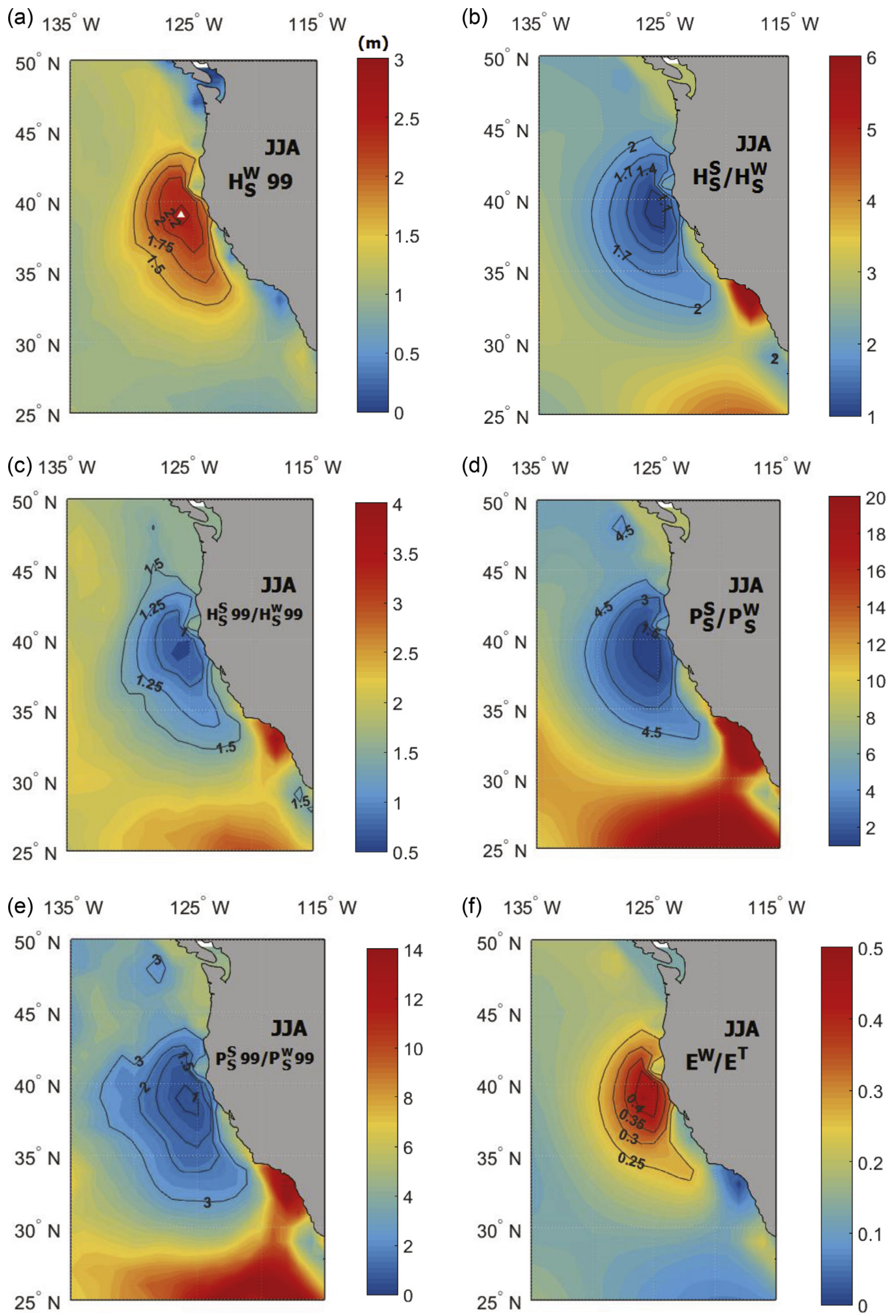

Fig. 4. California EBC, JJA (a) climatological mean H_s^w99% percentile, climatological distribution of the (b) mean H_s^s/H_s^w (dimensionless), (c) mean $H_{s99\%}^s/H_{s99\%}^w$ (dimensionless), (d) mean P_w^s/P_w^s (dimensionless), (e) mean $P_{w99\%}^s/P_{w99\%}^w$ (dimensionless), and (f) and mean E^w/E^T (dimensionless).

percentiles, and the mean wind sea spectral energy weight at the surface E^w/E^T (where E^w and E^T are wind sea and total spectral density energies, respectively), are shown.

The swell and wind sea wave energy fluxes (or power, in watts per linear wave crest meter; w m^{-1}) are defined as:

$$P_w^s = \frac{\rho g^2}{64\pi} T_m^s (H_s^s)^2, \tag{2}$$

Table 1
Geographic positions of key points in each area of interest (see white triangles on panels a. on Figs. 4–8), referred to the respective H_s^w99% percentile summer maxima.

Area	Position key point
California	39° N −126° W
Canary	31° N–12° W
Humboldt	35° S–74° W
Benguela	27° S–13° E
West Australia	28° S–111° E

Table 2
Summary of results at key points (white triangles on panels a. in Figs. 4–8; positions in Table 1) – seasonal mean values, with the exception of H_s^w99%.

Area	H_s^w99% (m)	H_s^s/H_s^w	$H_{s99\%}^s/H_{s99\%}^w$	P_w^s/P_w^s	$P_{w99\%}^s/P_{w99\%}^w$	E^w/E^T
	JJA					
California	2.4	0.99	0.79	1.03	0.83	0.44
Canary	1.7	1.09	0.89	1.41	1.13	0.43
	DJF					
Humboldt	1.9	1.76	1.36	4.03	3.01	0.26
Benguela	1.9	1.40	1.18	2.47	2.08	0.33
W. Australia	2.0	1.54	1.24	3.18	2.32	0.30

$$P_w^w = \frac{\rho g^2}{64\pi} T_m^w (H_s^2)^2, \tag{3}$$

respectively, where ρ is the sea water density, and g is the gravitational acceleration.

The H_s^w 99% percentile ($H_{s99\%}^w$; Fig. 4a) can reach values consistently higher than 2 m offshore California. The maximum value is 2.4 m, at the location marked as a white triangle. On each area a key point is chosen, using the $H_{s99\%}^w$ maximum value (see Table 1 for geographic positions). See also Table 2 for the $H_{s99\%}^w$ maximum values. These extreme locally generated waves, occurring about 1% of the time, are steep waves with short wavelengths (and periods; not shown), covering an area spanning from about 34°N to 44°N, with an offshore extend of about 800 km. These waves are the result of locally intensified extreme wind speeds (also not shown), that have grown rapidly in a limited fetch dimension. Coast parallel winds along the EBC systems, in summer, are primarily intensified by the ocean-land temperature contrast at the coast, but also due to the interaction of the flow with the coastal orography. The warm subsiding air from the subtropical high-pressure systems above and the cold marine air at the surface, origin sharp temperature inversions that cap the MABL at the coast, constraining the flow and the wind speed maxima at lower altitudes. The temperature decrease of the marine layer along the coast, due to the upwelling and low SST, is further responsible for the sloping of the capping inversion towards the coast. The increase of the wind speed nearshore, in summer, along the coastal areas above the five EBC systems, is therefore the result of channelled flow, with a temperature inversion above (at ~400 to 500 m; Ranjha et al., 2013, Soares et al., 2014, Rijo et al., 2017), a sharp pressure gradient from the ocean to the coast, and, most of the times, a mechanical constraint imposed by the coastal topography (Winant et al., 1988; Burk et al., 1999, Ranjha et al., 2015b). The low level coastal atmospheric flow along the EBC systems can also be intensified by the coastal topography and orientation (Burk and Thompson, 1996; Tjernström and Grisogono, 2000), resulting in additional local enhancement of the wind speed through a process called expansion fan in the lee of capes and headlands (Winant et al., 1988). This local enhancement of the wind speed is, despite the coarse resolution, captured by the ERA-Interim (Ranjha et al., 2013, 2015a), with a direct impact on the wind sea waves field, as seen in Fig. 4a, where a bubble shaped area of intensified H_s^w occurs south of central California coastal headlands. When compared to the mean swell heights in the same area (Fig. 4b), the mean summer H_s^w can be, in the core of the intensified wind sea heights, practically the same as H_s^s (where $H_s^s/H_s^w \cong 1$; see Table 2), which is a rare situation in the global ocean (Figs. 2 and 3, and Semedo et al., 2011). When looking at the comparison between the summer extreme swell (H_s^s 99% percentile: $H_{s99\%}^s$) and wind sea wave heights (Fig. 4c) it can be seen that extreme wind sea heights, offshore the coast of central California, are now higher than swell heights ($H_{s99\%}^s/H_{s99\%}^w \cong 0.8$). This occurs, given the proper conditions, due to headland intensification of the local wind speed, and then to the intensification of the locally generated waves, that become higher than the remotely generated ones. It must be understood, nevertheless, that this is the effect of several interconnected processes: the synoptic pattern (subtropical high and thermal low) that aligns the along coast wind with the coastal headlands, the low STT at the coast that sharpens the coastal wind speed, and the low swell wave heights, which, in the summer, can originate in the northern and southern hemisphere.

The wave energy flux (or the ability of waves to actually perform work), is a function of the wave heights, to the second order, but also of the wave periods, to the first order. Hence, for equal wave heights, longer waves carry more energy per wave crest unit length Eqs. 2 and (3). The ratio between the swell and wind sea wave energy fluxes (Fig. 4d) shows that, despite the long swells reaching the area, the locally generated wave energy flux is, on average, comparable, i.e., $P_w^s/P_w^w \cong 1.5$ (1.03 at the peak; see Table 2). It is worth mentioning the combination of the sheltering effect of the Southern California Bight and the intake of long swells from the south (most probably from the southern hemisphere), rising P_w^s/P_w^w to values close to 20 or more. The situation slightly changes when the summer swell and wind sea wave energy fluxes extreme values are compared (Fig. 4e) through the ratio between the swell and wind sea 99% percentiles ($P_{w99\%}^s$ and $P_{w99\%}^w$, respectively). Now extreme wind sea wave heights, although short in length, can carry more energy than swell waves under extreme situations ($P_{w99\%}^s/P_{w99\%}^w < 1$). During about 1% every summer (ca. 1 day per summer) extreme locally generated waves, consistently higher than 2 m height, short, but highly energized, can occur offshore central California, having a high destructive capability and posing a serious threat to the local navigation and ocean related seasonal tourism. Still having in mind wave energy, and how it is distributed by wind sea and swell waves along the California EBC, the mean wind sea spectral zeroth moment (m_o^w), and the total mean spectral moment (m_0), were computed, with the goal of assessing the summer mean wind sea energy density (E^w) weight. The zeroth wave spectral moment is defined as

$$m_0 = \iint f^0 F(f, \theta) df d\theta, \tag{4}$$

and m_o^w was computed by integrating the spectra from the separation frequency $\hat{f}$ to the highest frequency in the wave model frequency range (and from 0° to 360° in direction). The wave (density) spectral energy content (or energy spectral weight, as called by Semedo et al. (2011)) of the wind sea was computed as the ratio $E^w/E^T = m_0^w/m_0$, where E^T is the total wave energy density It should be noted that $E^w/E^T = 1 - E^s/E^T = m_0^s/m_0$, where E^s is the swell energy density, and m_0^s is the swell spectral zeroth moment, computed by integrating the spectra from lowest frequency in the frequency range and separation frequency $\hat{f}$, and from 0° to 360° in direction. The summer mean wind sea spectral weight offshore California (Fig. 4f), shows that the wind sea part of the spectra is, on average, less that the swell one. The JJA mean E^w/E^T maximum value is close to 0.5, but less than that in most of the area, meaning that at its maximum wind sea accounts for about half of the wave energy in the mean wave spectra. Nevertheless, these values are within a range of 0.3–0.5, making the locally generated wave energy slightly lower and comparable to the one generated remotely, which is an uncommon feature along the world oceans, as shown by Hanley et al. (2010) and Semedo et al. (2011).

In Fig. 5 the same statistics shown for the coast of California-Oregon, are presented for the Canary EBC in JJA, covering an area along Iberia, Morocco, and Western Sahara. The $H_{s99\%}^w$ along the Canary

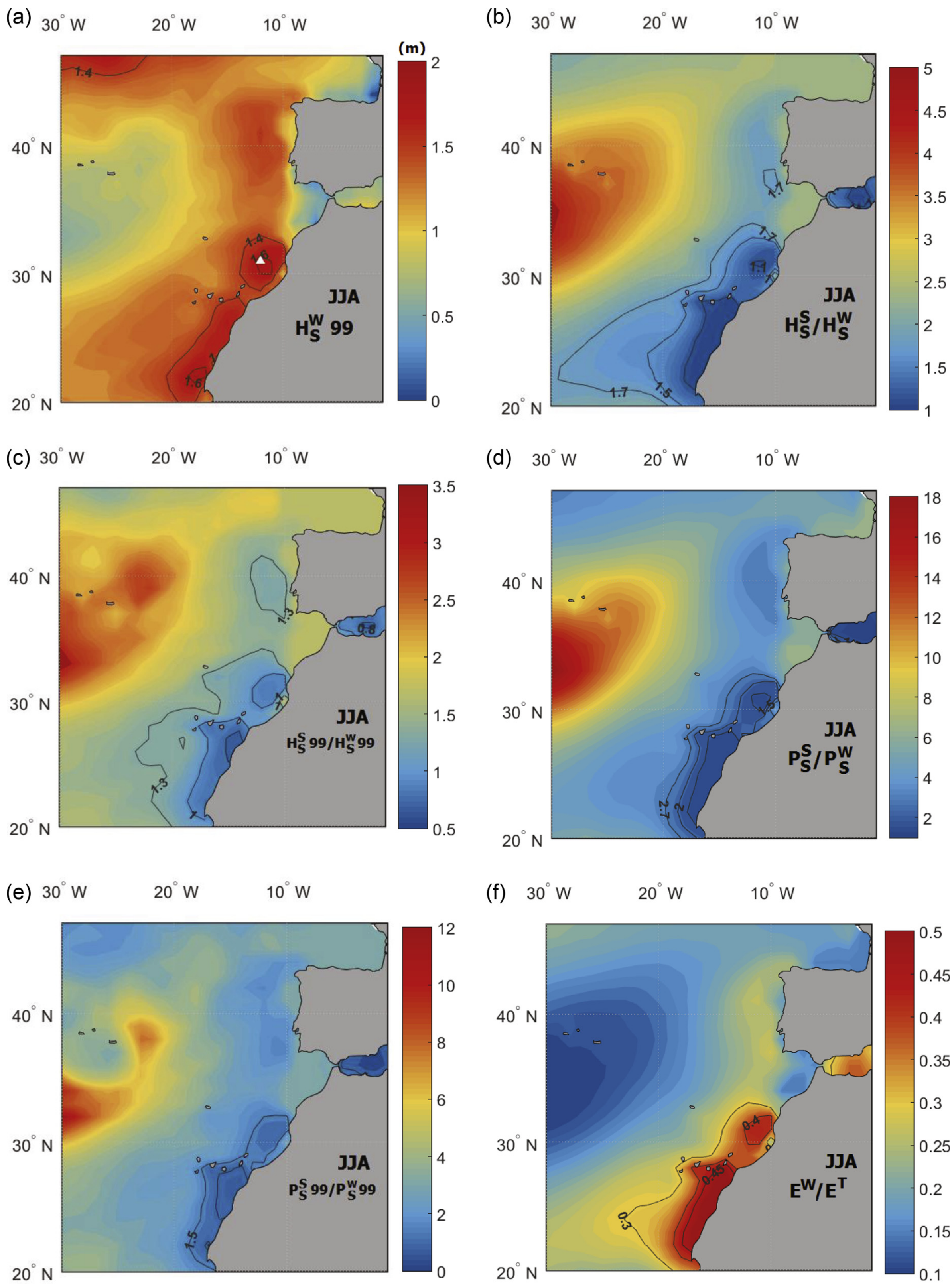

Fig. 5. Same as in Fig. 4 but for Canary EBC in JJA.

current (Fig. 5a) shows different values from offshore west Iberia to Northwest Africa, with a clear separation between these two areas defined by the Gulf of Cadiz, where locally generated waves decrease. The extreme wind sea wave heights are lower along Iberia (~1–1.2 m) compared the ones west of Morocco and Western Sahara (~1.4–1.6 m, reaching a maximum of 1.7 m; see Table 2), and lower overall than along the California EBC. Mean (Fig. 1a) and extreme wind speeds (not shown) are higher offshore California, compared to Iberia and Northwest Africa (Ranjha et al., 2013), and for that reason mean and extreme wind sea wave heights are also higher there. The wind speed is intensified in the lee of several capes, mostly along the coast Morocco and Western Sahara, with a direct impact on the locally generated waves. When summer wind sea and swell wave heights are compared (Fig. 5b; H_s^s/H_s^w), only offshore Western Sahara H_s^w becomes comparable to H_s^s (despite H_s^s/H_s^w being always higher than 1, with a minimum value of 1.09; see Table 2), with values similar to the offshore California ones. This happens due to the local intensification of the wind speed driven by the interaction of the flow with the coastal orography. This wind speed intensification has a direct impact on the raise of the locally generated wave heights that become, in JJA, comparable to the remotely generated ones. The local comparison between the JJA swell and wind sea extreme wave heights (Fig. 5c; $H_{s99\%}^s/H_{s99\%}^w$) along Canary Current shows that, particularly in the lee of major capes in Morocco and Western Sahara, extreme wind seas are higher than the swells, although lower, comparably, than in California. Along western Iberia $H_{s99\%}^s/H_{s99\%}^w > 1$, since not only extreme wind sea waves are lower there than in Africa, but also swell wave heights are higher.

The unique characteristic of the wind and wave fields long the Canary EBC, compared with the remaining four EBC, should be noted. Not only the Canary Current is disrupted by the influx of Mediterranean (denser) water into the North Atlantic basin, sinking as if flows through the Gibraltar Straight, but also interacting with the equatorward surface flow (Pastor et al., 2015), but also the coast line is also different from other continental mid-latitude western coasts. The Gulf of Cadiz disrupts the coast south of Portugal, and the flow encounters open waters situations, finding coastal environment some hundreds of kilometers south, in Northwest Africa. Therefore, two separated centers of action exist along the Canary Current: along Western Iberia, and along the Northwest African coast. This fact was also mentioned by Ranjha et al. (2013), which separated the Canary coastal jet in two: the Iberian Coastal jet and the North Africa coastal jet.

From the comparison between the swell and wind sea wave energy fluxes in JJA (Fig. 5d) it can be seen that, despite the local intensification of the wind speed, as in California, swell waves along the Canary EBC still carry, on average, more energy than the former, with values of the ratio $P_w^s/P_w^w > 1.5$ (1.41 at its minimum; see Table 2). The higher mean values of P_w^s/P_w^w (representing less wind sea energy flux) take place are along West Iberia. When summer extreme values of swell and wind sea wave energy fluxes are compared (Fig. 5e), $P_{s99\%}^w$ values are closer to $P_{s99\%}^s$, particularly along the coasts of Morocco and Western Sahara, but still remotely generated waves carry more energy than the local ones (which is not the case along the California EBC, where in extreme events $P_{s99\%}^s/P_{s99\%}^w \cong 1$). Nevertheless, in extreme situations, mostly along the Northwest coast of Africa, severe wind speed events can lead to extreme locally generated wave heights, carrying considerable amounts of energy. The wind sea wave energy density weight (Fig. 5f) is about the same as in California: close to 0.4 at its peak along the Western Sahara coast. The sheltering effect of the Canary Islands limits, to a certain extent, swell energy density content there, while the local intensification of the wind speed, due to the interaction of the flow with the coastal headlands, increases the relative content of the wind sea energy density role.

Analogous statistics were also computed for the southern hemisphere EBC areas, for the Austral Summer. One of the characteristics of the winds along the southern hemisphere EBC, particularly along the Humboldt and Benguela currents, is their lower seasonality, compared to the northern hemisphere (Ranjha et al., 2013; Lima et al., 2018). Hence, besides DJF, relevant wind sea waves are expected to be generated there in MOM and SON (not shown), but also during the Austral Winter (Figs. 1b and 2).

The summer wave field statistics along the Humboldt EBC are shown in Fig. 6. The mean extreme wind sea wave heights (Fig. 6a; $H_{s99\%}^w$) there, are, at its peak, of the order of 1.8–1.9 m (see Table 2): lower than offshore California, but comparable to the Canary EBC area. The local intensification of the wind speed due to the interaction of the flow with coastal topography has also been previously documented (Muñoz and Garreud, 2005; Garreud and Muñoz, 2005), and has a direct impact on the wind sea wave heights locally. The comparison between the mean DJF wind sea and swell wave heights (Fig. 6b; H_s^s/H_s^w) reveals that, contrary to what happens along the northern hemisphere EBC areas, offshore Chile, the wind sea wave heights are lower that the swell ones, therefore H_s^s/H_s^w is always clearly higher than 1 (1.76 at its peak; see Table 2). The Southern Ocean wind speed and wave height seasonality is lower than in the northern hemisphere (Figs. 1–3). For that reason, despite the clear local generation of wind sea waves in summer along the Humboldt EBC, waves keep being generated along the Southern Ocean storm belt, in the Pacific and Indian Sectors, propagating northward as swells and reaching the coast of Chile. So, in that area, the mean wind sea wave heights are clearly lower that the swell ones, making wave climate offshore Chile different from the equivalent areas in the northern hemisphere. The situation changes slightly when extreme wind sea and swell wave heights are compared (Fig. 6c; $H_{s99\%}^s/H_{s99\%}^w$). Now the local extreme waves are more comparable to the swell extreme wave heights, but still $H_{s99\%}^s/H_{s99\%}^w > 1$ (1.36 at its peak; see Table 2) is the overall situation, which is, still, different from what occurs in the northern hemisphere, once again due to the strong swell intake.

The Southern Ocean swell effect along the Humboldt EBC in DJF is even more pronounced when the swell and wind sea wave energy fluxes are compared (P_w^s/P_w^w; Fig. 6d). Longer and still relatively high swell, therefore carrying a great amount of energy, reach the area. The wind sea wave energy flux, when compared to the swell power, is clearly lower, and $P_w^s/P_w^w > 4$. This ratio is different from the northern hemisphere, where the locally generated wave energy flux is comparable to the swell one. The total wave energy flux offshore Chile (not shown) is also higher than along the California and Canary currents. The extreme wind sea and swell energy fluxes are more comparable (Fig. 6e) than their respective means, although remotely generated waves still dominate energy wise, compared to the locally generated ones. The ratio of the swell and wind sea wave energy fluxes 99% percentiles ($P_{s99\%}^s/P_{s99\%}^w$; Fig. 6e) shows that swell waves power is still 3–3.5 times higher than wind sea waves (with a minimum value of 3.01; see Table 2). A similar pattern occurs when looking at the DJF wind sea energy spectral weight (E^w/E^T; Fig. 6f), which is lower, compared to similar patterns along California, and Iberia and Northwest Africa. The wind sea energy spectral weight in this region is, at its peak, of the order of 30%, and less than that in most of the area offshore Chile. Swell waves, generated far in the Pacific extratropical storm tracks thus have a higher role along the Humboldt EBC, in terms of energy, compared to the locally generated waves, and in comparison to the northern hemisphere.

As in the Humboldt current, Benguela has two characteristics differentiating it from the northern hemisphere EBC. On the one hand, the coastal winds offshore Namibia and South Angola have a lower seasonality (Ranjha et al., 2013; Patricola et al., 2016; Lima et al., 2018), with a considerable occurrence of coastal low level jets, almost all year round (Lima et al., 2018). On the other hand, the South Atlantic, as in the Indian and Pacific Oceans, is still very active storm wise in summer, with considerable wave generation activity (Figs. 1–3). Nevertheless, the South Atlantic has some unique characteristics that make it different from the South Pacific. The narrow Drake Passage prevents most of the South Indian and Pacific Oceans swell to penetrate the South Atlantic (which is not the case of the Pacific Ocean, that receives swell waves from the South Indian Ocean; Young, 1999; Alves et al., 2003; Semedo et al., 2011), and the South Atlantic storm activity and strength (and wind speed) are less intense than their Indian and Pacific Ocean counterparts (Fig. 1). Fig. 7 depicts the Benguela EBC wave climate statistics. The extreme wind sea wave heights ($H_{s99\%}^w$) shown in Fig. 7a are similar to the Humboldt EBC (~1.7–1.8 m). On the other hand, since the intake of South Atlantic swell into the area is lower, the DJF mean wind sea and swell wave heights ratio (Fig. 7b; H_s^s/H_s^w) is slightly lower (1.4 minimum value; see Table 2) than offshore Chile, revealing a higher contribution of locally generated waves. As in the remaining

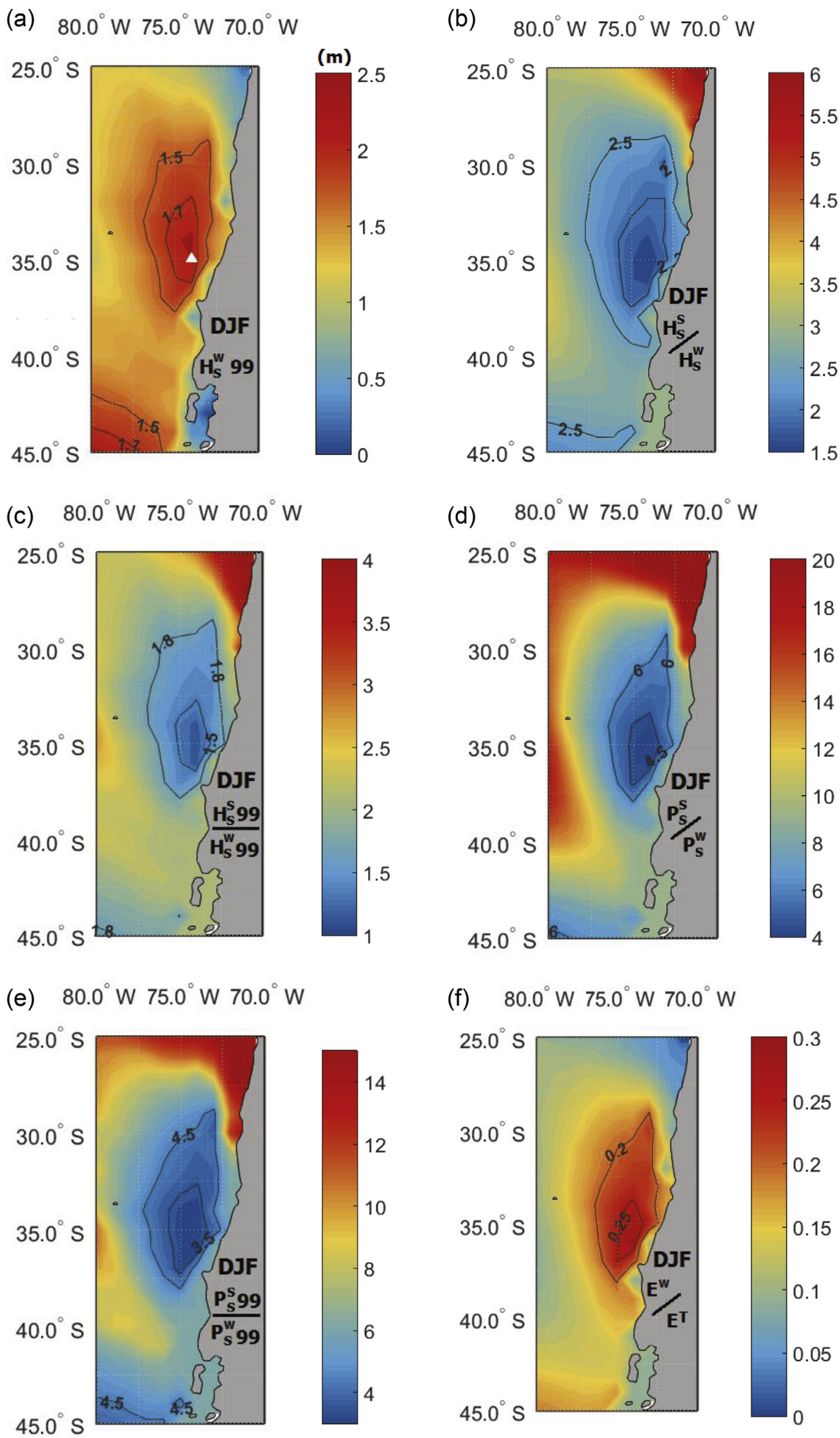

Fig. 6. Same as in Fig. 4 but for Humboldt EBC in DJF.

EBC, the local intensification of the wind speed along the Benguela Current due to the interaction with costal morphology (Nicholson, 2010; Patricola et al., 2016) contributes to the increased role of the locally generated waves, seen also in the comparison between extreme wind sea and swell waves (Fig. 7c; $H^s_{s99\%}/H^w_{s99\%}$) with values close to 1, lower than offshore Chile (1.4; see Table 2). This effect is not enough to raise the wind sea wave energy flux to the same level of the swell power in the area. Nevertheless, swell and wind sea energy fluxes are more comparable (Fig. 7d) along the Benguela EBC than offshore Chile, with $P^s_w/P^w_w \sim 3$ (2.47 minimum; see Table 2), which is lower than along the

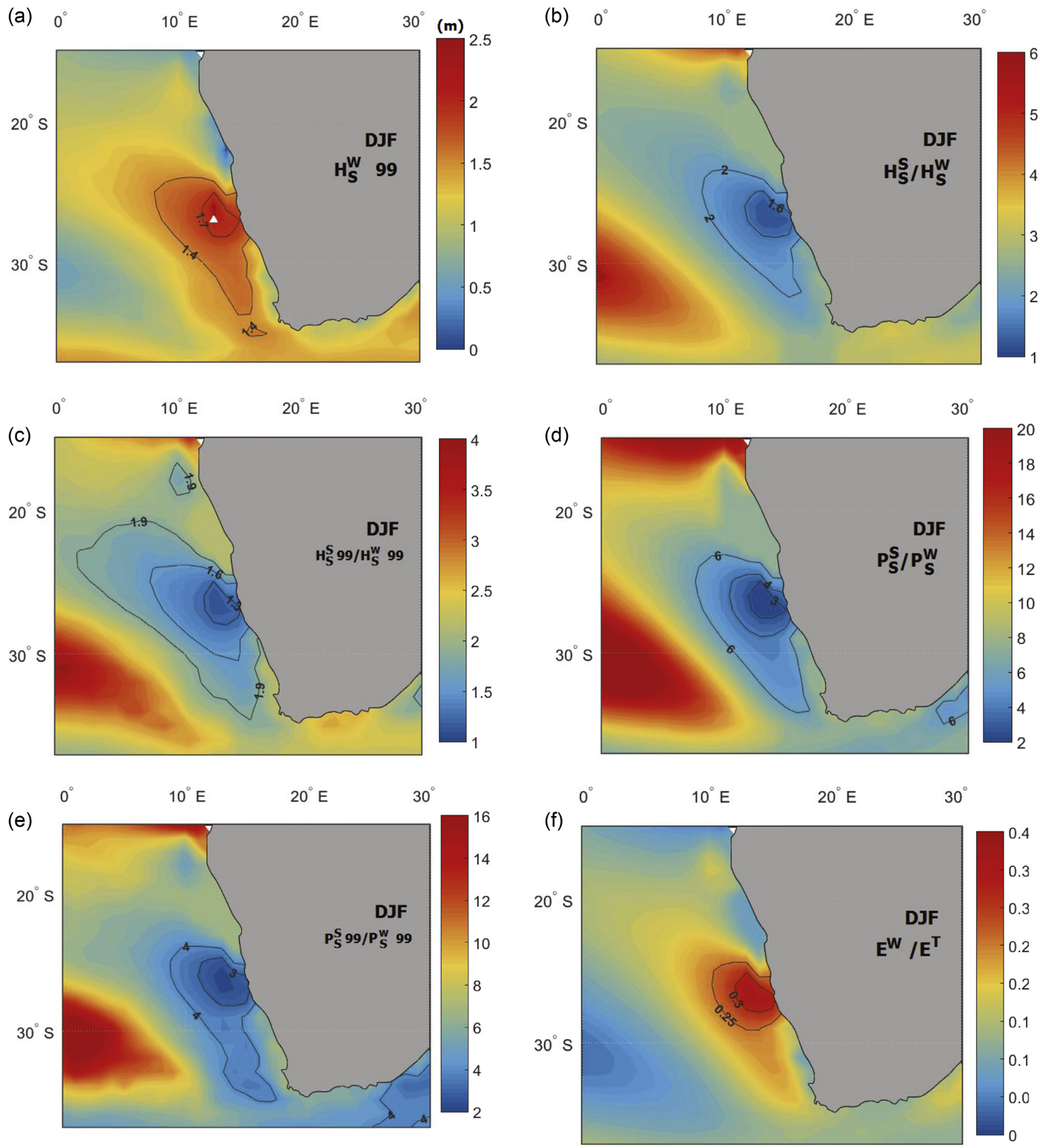

Fig. 7. Same as in Fig. 4 but for Benguela EBC in DJF.

Humboldt EBC, and closer to the California and Canary currents. The results of the comparison between the extreme swell and wind sea wave fluxes (Fig. 7e, $P^s_{s99\%}/P^w_{s99\%}$) are very similar the mean values comparison, with extreme swells transporting around at least twice more energy (2.47 at the peak; see Table 2) than extreme locally generated waves. The DJF wind sea wind sea energy spectral percentage (Fig. 7f; E^w/E^T) is very similar to the one in Chile (30–35%), and lower than the EBC currents in the northern hemisphere.

The Indian Ocean wave climate has also some distinctive characteristics, compared to the Pacific and the Atlantic Oceans. Its north span ends in the Arabian Sea at around 20°N, and it has only one main wave generation area, in the south extratropical storm tracks. On the other hand, the highest mean wave heights in the global ocean occur in the Southern Indian Ocean (while the most extreme wave heights occur in the North Atlantic sub-basin; not shown). In JJA, the mean H_s along the Southern Ocean storm belt (Indian Sector) reaches mean values of the order of 6 m (Fig. 2a), and in DJF these values are still high, with mean H_s higher than 4 m (Fig. 2b). These waves

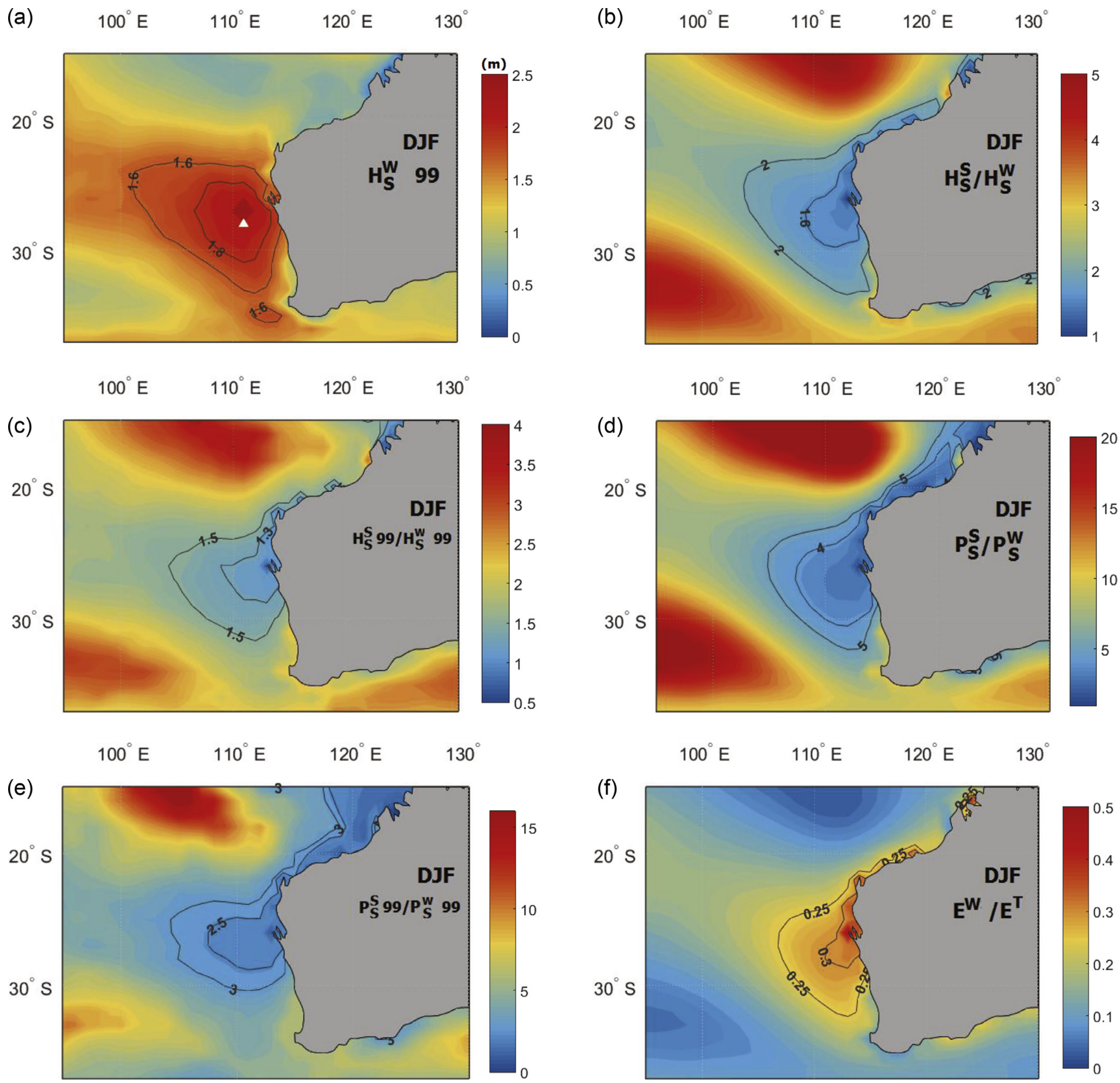

Fig. 8. Same as in Fig. 4 but for West Australia EBC in DJF.

propagate eastward as swell all year round, but also northward, literally propagating wave energy across the entire Indian Ocean basin (Figs. 2b and 3b). These swells also reach the West Australia coast, where local waves are generated due to the summer wind speed increase, as in the remaining EBC areas. The DJF statistics of the balance between wind sea and swell waves offshore west Australia, the last of the five EBC depicted here, are shown in Fig. 8. The extreme locally generated summer waves along west Australia (Fig. 8a; $H^w_{s99\%}$) are almost as high the California EBC ones (2.0 m maximum; see Table 2). Opposite to what happens along the other two southern hemisphere EBC, winds offshore west Australia have a well-defined seasonality (being virtually absent in winter), and are also slightly stronger than along the coasts of Chile and Namibia-Angola. For these reasons, despite the high mean swell waves that propagate from the higher latitudes into the area, mean locally generated wave heights are still comparable to those, with H^s_s/H^w_s values of the order of 1.5 (Fig. 8b), similar to Humboldt and higher than in Benguela. When considering extreme local waves offshore West Australia they are now more comparable to extreme swells (Fig. 8c; $H^s_{s99\%}/H^w_{s99\%}$). Extreme wind speeds contribute to these high locally generated waves, reaching heights close to swell waves, where $H^s_{s99\%}/H^w_{s99\%}$ shows values closer to 1 (1.24 at its peak; see Table 2), lower than along Humboldt EBC and similar to offshore Namibia-Angola. Long swell waves, generated southward, are still more energized, carrying, on the mean, more energy than local waves (Fig. 8d), since $P^s_w/P^w_w \sim 3$ or higher. When extreme waves are considered (Fig. 8e, $P^s_{s99\%}/P^w_{s99\%}$) these values are lower (2.3 at its peak; see Table 2). The West Australia wind sea wind sea energy spectral percentage (Fig. 8f; E^w/E^T) is of the order of 25–30%, which is comparable to the Humbolt and Benguela EBC areas, but lower than along the California and Canary EBC currents.

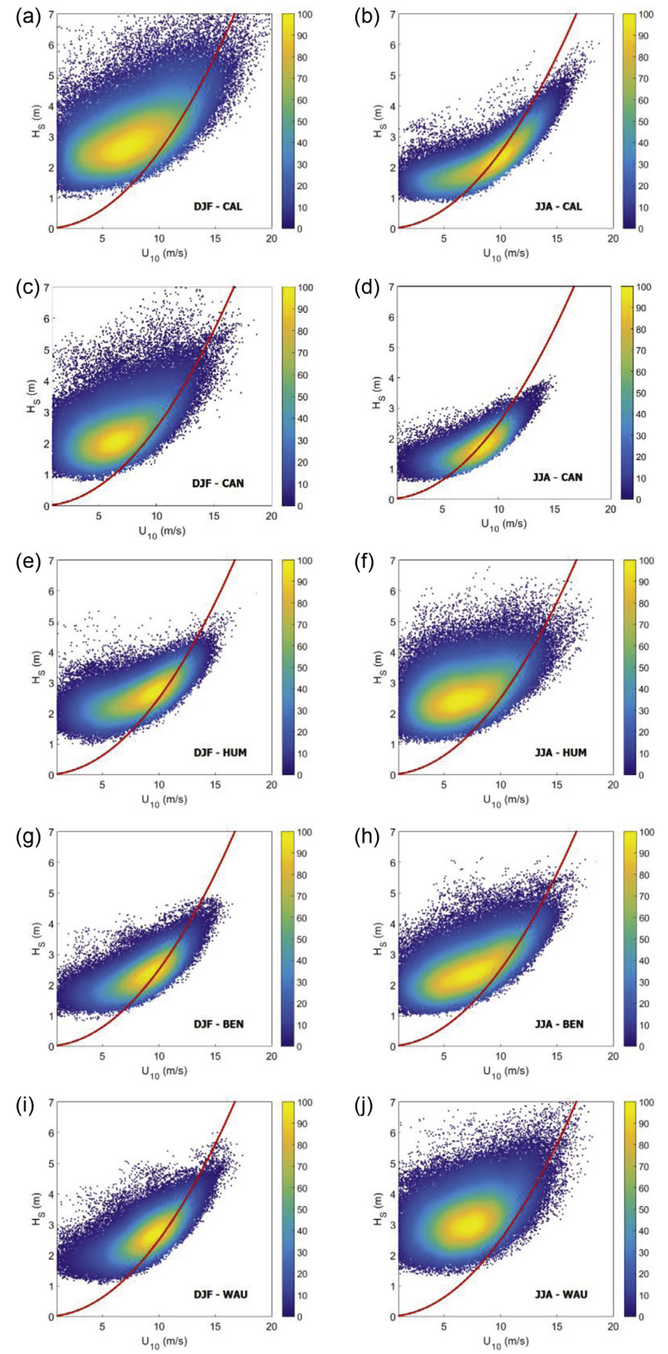

Fig. 9. Scatter diagrams of H_s (m) and U_{10} (ms^{-1}) for the respective key points (see Table 1 and white triangles on panels a. on Figs. 4–8) and 8 grid points around it for California EBC in (a) DJF and (b) JJA, Canary EBC in (c) DJF and (d) JJA, Humboldt EBC in (e) DJF and (f) JJA, Benguela EBC in (g) DJF and (h) JJA, and West. Australia EBC in (i) DJF and (j) JJA. The overlaid red lines represent the Pierson Moskowitz theoretical relation between U_{10} and H_s, a defined in Eq. (5), for fully developed seas.

Summer and winter scatter diagrams of H_s and U_{10} are shown in Fig. 9 for the five EBC. The scatter plots are built for the respective DJF and JJA season, from specific key points (marked as white triangle on panels a. in Figs. 4–8) and the 8 grid points around them. The key points were chosen considering the peak values of $H^w_{s99\%}$ at each area, during the correspondent summer, and are seen as representative extreme summer wind sea positions of the respective areas. The Pierson Moskowitz fully developed seas empirical relation, between U_{10} and H_s, is also shown in each scatter plot. This empirical relation, found by Pierson and Moskowitz (1964), and further corrected by Alves et al. (2003), defined as:

$$H_s = 0.025U_{10}^2, \quad (5)$$

is shown as a red line in the scatter plots. The fully developed relation (line) can be seen as a separation between the wind sea and swell sea states: the U_{10} and H_s pairs under the line represent developing seas, where wind sea dominates, and the ones above are considered swell dominated seas, with wave ages lower and higher than 1.2, respectively. According to the wave growth theory U_{10} and H_s follow a monotonic relation at the growing sea state (Koeman et al, 1994), until a fully developed spectrum, corresponding to a saturated level is achieved. The equilibrium (saturated) state, represented by Eq. (5), is an asymptotic state, where the wave spectrum is fully developed, and from then on only its shape and peak frequency are changing slowly in time. The wave age parameter is defined as c_p/U_{10} (where c_p is the peak wave phase speed). From Eq. (5), and from the Pierson and Moskowitz spectral theory (Pierson and Moskowitz,1964), it can be demonstrated that the fully developed sea state corresponds to a wave age of 1.2, where $c_p = 1.2U_{10}$ (Holthuijse, 2008; Alves et al., 2003; Semedo, 2010; Semedo et al., 2012; Högström et al., 2011).

The higher levels of scattering at the five areas, in the respective winters (Fig. 9a,c for California and Canary, and Fig. 9f,h,j for Humboldt, Benguela, and West Australia), and the highest density of points clearly above the respective fully developed seas lines, emphasizes the dominant presence of swell (or remotely generated waves). Interestingly, despite the distance between the areas of interest, the shape of the scatter plots is rather similar, indicating the same type of winter sea state regimes. The California EBC has a higher dispersion of the (H_s, U_{10}) pairs, and a different scatter plot shape (Fig. 9a), due to the presence of northern and southern hemisphere swells. The open shape of the Pacific Ocean and to the strong wave generation activity in the Southern Ocean, even during the Austral Summer allows the arrival of swells from both hemispheres in DJF to the coast of California. During JJA, in the California and Canary EBC areas, the situation changes significantly: the dispersion is much lower, with more points concentrated in the vicinity and below the fully developed line, revealing a wind sea dominated sea states. The situation in the northern hemisphere, during the Boreal Summer, is different from the southern hemisphere, since the extratropical storm activity is low, and the high wind speed events do occur but along the two EBC, giving rise to strong wind sea dominated sea states offshore California and (mostly) Morocco and West Sahara. Nevertheless, some swell waves, generated in the southern hemisphere, propagate into California in JJA, hence in this area the number of points above the fully developed seas line is higher (as is the dispersion). During DJF, along the Humboldt, Benguela, and West Australia EBC, the scattering is lower than in JJA, with a higher number of points on the wind sea dominated side. The dispersion of the (H_s, U_{10}) pairs in these three areas, although lower than in winter, is higher than in the two northern hemisphere areas. This occurs due to the low seasonality of the wave climate in the southern hemisphere, with waves being generated in the extratropical latitudes even in summer, which propagate into the coasts of Chile, Namibia-Angola, and West Australia.

3.3. Intra-annual variability

Fig. 10 displays the intra-annual variability (monthly means) of the close to surface wind speed (U_{10}), significant wave heights (H_s, H_s^s, and H_s^w), and mean wave periods (T_m, T_m^s, and T_m^w), at 9 grid points: at the 5 key points in each EBC area plus the 8 grid points around them). The intra-annual variability of U_{10} in the five key points shows a gradual increase of the local wind speed during the hemisphere summer. This increase is more defined in the California and Canary currents, and in the West Australia current. Along these areas, a clear peak in July, for

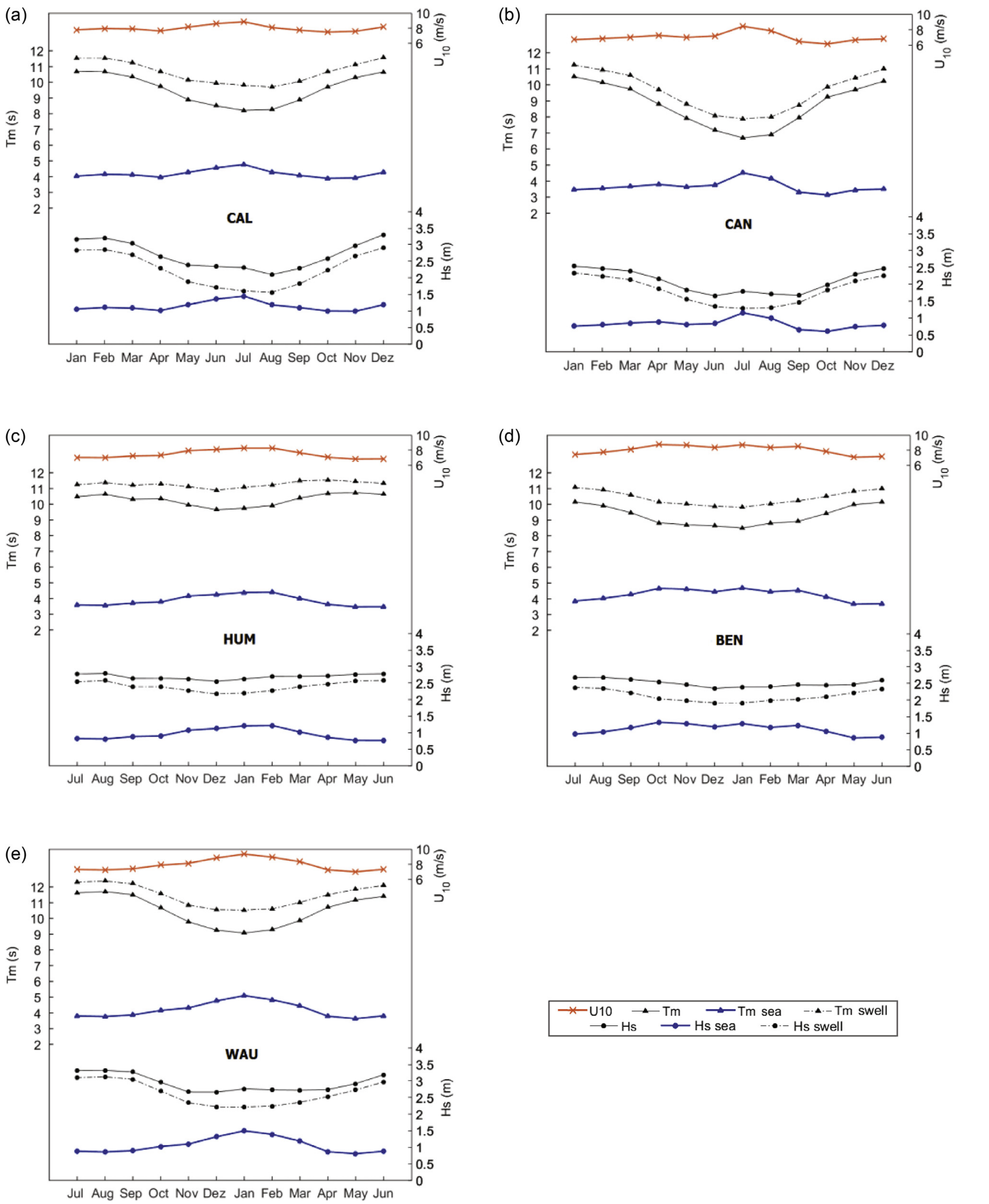

Fig. 10. Intra-annual variability of U_{10} (ms^{-1}; red line with "x" at upper right scale), T_m, T_m^s and T_m^{ws} (s; black full line, black dashed lie, and black dashed dot line, with full triangles, respectively, at central left scale), and H_s, H_s^s and H_s^w (m; blue full line, blue dashed lie, and blue dashed dot line with full circles, respectively, at bottom right scale), averaged for the respective key points and 8 grid points around (see Table 1 and white triangles on panels a. in Figs. 4–8) for (a) California EBC, (b) Canary EBC, (c) Humboldt EBC, (d) Benguela EBC, and (e) Western Australia. (For interpretation of the references to colour in this figure legend, the reader is referred to the web version of this article.)

the northern hemisphere areas, and January, for West Australia, can be seen, corresponding to the highest summer mean wind speed. This summer increase is lower and more gradual offshore Chile and Namibia, with a less defined mean wind speed increase, and highest wind speeds occurring during 4 months (from November to February) in the Humboldt EBC, and virtually for 6 months in the Benguela EBC (from October to March). Not surprisingly the H_s^w and T_m^w intra-annual variabilities, at the five areas of interest, show a very high correlation with the close to surface wind speed inter-annual variability (>0.95). In the California and Canary areas, the mean H_s decreases during summer, as does H_s^s. Nevertheless, the decrease in H_s is lower than the swell heights, due to the effect of the locally generated waves, that are higher during summer, balancing the decrease ofH_s^s. In the Canary EBC, during July, the mean H_s actually increases, due to the increase of the mean July H_s^w, since the H_s^s also decreases during that month. In July, the mean values of H_s^w, offshore California and the Atlantic coast of Morocco, is almost the same as H_s^s. A similar behaviour and relation can be found in the West Australia EBC, with the peak of H_s^w taking place in January. Nevertheless, in this area the mean H_s^w is always lower than H_s^s, despite the fact that locally generated waves do drive the slight increase tendency of the mean H_s during the austral summer, opposite to the H_s^s behaviour. The intra-annual variability of the wave heights offshore Chile and Namibia is different from the remaining three areas. In these two regions, the mean H_s^s variation throughout the year is very low. Despite the increase of the locally generated wave heights during part of the year (cantered in the austral summer months), it has a low effect on the annual cycle of H_s, which ends up being more controlled by the all year round impinging swells.

4. Discussion

As shown in the previous section, the effect of the summer intensified wind speeds on the local wave field, along the five EBC, is notorious. Along these five areas, the ratio between the swell and wind sea wave heights (H_s^s/H_s^w) decreases in summer, due to the rise of the locally generated wave heights. This increase is also reflected in the higher energy content of the local waves during summer, as well as in extreme locally generated wave heights (summary in Table 2). The effect of the summer local winds in the local wave field is similar between the five regions, nevertheless some differences prevail, due to the intake of swell waves, but also due to the different wind speed seasonal variabilities, as shown in Fig. 10. A clear indicator of these differences can be seen on Fig. 9, from the dispersion along the fully developed seas line, during summer. The dispersion of the (H_s,U_{10}) pairs is lower in summer (compared to the respective winter): lower in the California and Canary EBC, compared to the remaining southern hemisphere EBC. This dispersion has been assessed by computing the percentage of (H_s,U_{10}) pairs above and below the fully generated seas line, but also by computing the mean distance to this line for the points above and below the line (where positive values represent the former and negative values the later). Additionally, the standard distance (SD) of the (H_s,U_{10}) scatter distribution has been computed. The standard distance measures the compactness of a distribution, providing a single value (a distance) representing the dispersion around the centre, computed as

$$SD = \sqrt{\frac{\sum_{i=1}^{n}(H_{si} - \overline{H}_s)^2}{n} + \frac{\sum_{i=1}^{n}(U_{10i} - \overline{U}_{10})^2}{n}}, \tag{6}$$

where n is the number of events, in this case 460,188 (9 points times 12,783 days, in the 1979–2013 period, time 4 outputs per day), and $\overline{H}_s$ and $\overline{U}_{10}$ are the mean values of the SWH and wind speed at 10 m. These statistical parameters have been computed (for JJA and DJF) for nine grid points, centred at each area respective key point (see white triangle on panels a. in Figs. 4–8, and geographic positions in Table 1), and can be seen on Table 3. The California EBC (mostly on the Norwest African sector) area stands out as the area where, in summer, locally generated waves are highest, more extreme, and carry more energy (Fig. 4 and Table 2). Nevertheless, the summer wave field along the Canary EBC shows that wind sea dominated wave fields are more prevalent, compared to off-shore California and to the remaining southern hemisphere EBC areas. In JJA wind sea dominated wave events occur 48.4% of the times (Table 3a), when the (H_s,U_{10}) are under the fully developed curve (Fig. 9d) in the Canary EBC. This is in fact higher than in California (43.5% in JJA) and Humboldt, Benguela, and West Australia (20.3%, 27,9%, and 24.1%, respectively) in DJF, the southern hemisphere summer. Also along the Canary EBC the summer wave field is less scattered, i.e., more compact along the fully developed sea state and its mean (centre) value, since the mean distance of the swell and wind sea events to this curve are (0.53 and −0.31; Table 3b) are lower than in any other area, as is the standard distance (1.90; Table 3c). On the other hand, in DJF, wind sea events along the Canary EBC, off-shore Northwest Africa, are low (occurring only 8.1% of the times; Table 3a), which is lower than in California. West Australia is the EBC area with lowest wind sea dominated winter events (only 4.1% in JJA; Table 3a). This occurs because there is virtually no local wind in winter along West Australia (Fig. 1 and Ranjha et al., 2013).

Table 3
Summary of scatter plots results for each area of interest, at the respective key points (white triangles on panels a. in Figs. 4–8; positions in Table 1) and 8 adjacent grid points: (a) percentage of swell and wind sea points, (b) mean departures of swell and wind sea heights relative to the Pierson and Moskowitz fully develop seas curve (m), and (c) standard distance of H_s (m; see Eq. 5.). Summer (winter) refers to JJA (DJF) for the northern (southern) hemisphere areas and DJF (JJA) for the southern (northern) hemisphere ones.

Area	(a)	(b)	(c)
JJA			
California	56.5 / 43.5	0.84 / - 0.42	2.74
Canary	51.64 / 48.4	0.53 / - 0.31	1.90
Humboldt	91.7 / 8.3	1.61 / - 0.36	2.45
Benguela	87.4 / 12.6	1.35 / - 0.34	2.13
West Australia	95.9 / 4.1	1.89 / - 0.32	2.05
DJF			
California	87.0 / 12.9	1.74 / - 0.46	3.05
Canary	91.9 / 8.1	1.37 / - 0.27	2.44
Humboldt	79.7 / 20.3	1.10 / - 0.33	2.55
Benguela	72.1 / 27.9	0.81 / - 0.31	2.64
West Australia	75.9 / 24.1	0.86 / - 0.29	2.43

Although strikingly similar, as mentioned before, the characteristics of the southern hemisphere regional wave fields along the three EBC, have some differences compared to the California and Canary EBC areas. Summer (DJF) wind sea (swell) dominated events are lower (higher) than in the northern hemisphere. This occurs mostly due to the lower seasonality of the wind along the Southern Ocean storm belt (in the Pacific, Atlantic and Indian sectors), generating waves that propagate as swell even in summer, that reach the southern hemisphere EBC areas. For example, the mean wind speed along West Australia is relatively high in DJF: higher than along the Humboldt and Benguela, and comparable to the California in JJA (Figs. 1 and 10). Nevertheless, the swell intake in the Indian Ocean is so high, that prevents wind sea events to prevail in that area. To a certain extent the same occurs offshore Chile, and Namibia-Angola.

A summary of the mean H_s, H_s^s, and H_s^w values in the same nine grid points mentioned above (centered each area respective key point) for JJA and DJF, as well as for the respective summer months (June to August and December to February) are shown in Table 4. The mean H_s during Austral Summer, along the three southern hemisphere EBC, is higher than in California and Canary EBC areas in JJA. That occurs due to the intake of swell in the southern hemisphere, since in those three areas, in DJF, the mean H_s^s is considerably higher than the mean H_s^w there. The summer difference between H_s^s and H_s^w, along California and Canary EBC, is smaller. When looking at the mean monthly values, as in

Table 4
Mean H_s (m) H_s^s (m) and H_s^w (m) at key points (white triangles on panels a. in Figs. 4–8; positions in Table 1) and 8 adjacent grid points: for the northern hemisphere summer (JJA), and respective months (June to August), and for the southern hemisphere summer (DJA), and respective months (December to February). The results are presented only for the respective hemisphere EBC areas. NH is northern hemisphere and SH southern hemisphere.

NH areas	JJA	June	July	August
California	2.3 / 1.6 / 1.4	2.4 / 1.7 / 1.4	2.3 / 1.6 / 1.5	2.1 / 1.5 / 1.2
Canary	1.7 / 1.3 / 1.0	1.7 / 1.3 / 0.8	1.8 / 1.3 / 1.2	1.7 / 1.3 / 1.0
SH areas	DJF	December	January	February
Humboldt	2.6 / 2.2 / 1.2	2.6 / 2.1 / 1.3	2.6 / 2.2 / 1.2	2.7 / 2.2 / 1.2
Benguela	2.4 / 1.9 / 1.3	2.5 / 1.9 / 1.2	2.3 / 1.9 / 1.3	2.4 / 2.0 / 1.2
W. Australia	2.7 / 2.2 / 1.4	2.7 / 2.2 / 1.3	2.8 / 2.2 / 1.5	2.7 / 2.2 / 1.4

Fig. 10, clear peak monthly mean H_s^w values can be identified (June for California and July for Canary) in the northern hemisphere areas, which is not the case in the southern hemisphere areas, where the mean H_s^w is almost the same throughout the Austral Summer. The Summer mean H_s^woffshore Chile and Namibia-Angola is lower than in California, but higher than Along the California EBC. The Summer mean H_s along the West Australia is the highest of the five EBC areas, with the highest summer mean H_s^s, and the same mean H_s^w as in California.

5. Concluding remarks

A qualitative analysis of the wave climate over the mid-latitudes western coastal areas, along the five EBC systems, has been presented, based on the ERA-Interim reanalysis wave data. The analysis used the swell wind sea partition from the wave model WAM, and the swell and wind sea parameters available in ERA-Interim data set, as in e.g. Hanley et al. (2010) and Semedo et al. (2008, 2011, 2014). Despite the relatively coarse resolution of ERA Interim (0.7° in the atmospheric parameters and 1° in the wave parameters), it can be seen as an adequate data set, even in these coastal areas (Ranjha et al., 2013 and Lima et al., 2018), allowing a coherent relative comparison between the five areas of interest.

The strong seasonality of the coastal winds along the five EBC (Ranjha et al., 2013; Lima et al., 2018. and Fig. 1), has been shown to have a direct influence on the locally generated waves, triggering a peculiar regional wave climate:

- Strongly dominated by swell in the winter, when the local mean local wind speed is low; and
- High wind sea waves in summer, when the along coast wind speed increases and is responsible for the locally generated waves.

The locally generated waves along the EBC, in extreme wind speed situations, become high (of the order of 2–2.5 m; Table 2 and panels a. on Figs. 4–8), which can be seen as considerably high if we look at the areas downwind of capes and coastal headlands as limited fetch areas. Since these local waves are young waves, they are also relatively short lengthened, and hence rather steep (not shown), posing serious threats to coastal community seafarers, such as fishing vessels or summer tourism boating activity. It should be noted that the five main ocean upwelling systems lay exactly along the mid-latitude western coasts, due to the strong summer wind speed. These cold upwelled nutrient reach waters are responsible for the rich fishing resources, mainly in summer, when coastal fishing activity is stronger (Vallis, 2000; Leitão et al., 2014).

The direct effect of the summer intensified wind speeds on the local wave field, in the western mid-latitudes coastal areas, along the five EBC, has been studied. A qualitative study of the wave fields in these areas has been presented by comparing swell (remote) and wind sea (local) waves, quantifying their relative weight, not only in terms of their SWH, but also on their mean and extreme energy content. The H_s^w role, compared to H_s^s, in Summer, is highest than in any of the remaining four EBC areas. Offshore California extreme wind sea wave heights are highest (2.4 m), have almost the same mean height and mean wave energy flux as swell, and have the highest spectral weight of the five EBC areas (see Table 2.). Despite the distance between them, the wave climates along these five EBC areas are strikingly similar. For example the California EBC area wave field is rather similar to the Australia EBC one (Figs. 2 and 3 and Tables 2–4), where, for example, the summer mean H_s^w is the same, and the swell wind sea weight (H_s^s/H_s^w) is only lower in Australia because of the higher mean swell wave heights there. The reason for the similarities between the five areas lays in the fact that the atmospheric synoptic and regional scales responsible for the winds and waves (basin wide and regionally) share similar mechanisms. Although similar, the characteristics of the southern hemisphere regional wave fields along the three EBC, have some differences compared to the California and Canary EBC areas. These differences being due, mostly, to the lower seasonality of the Southern Ocean storm belt, generating waves that propagate equatorward as swell, even during the austral Summer, and defining regional and ocean basin scale wave climates.

A study of how waves impact the regional climates of the mid-latitude continental coastal areas, and consequent impact in-land, remains to be studied. It can be assumed that during summer, when wind sea waves are more prevalent, and the wave field is more prone to wave breaking and white capping, the wave induce turbulence further induced the mixing of the ocean surface layer. This mixing should therefore decrease the SST in the wind sea dominated areas (where the wind speed is highest) and contribute to the local thermal (pressure) gradient and ultimately to an increase of the wind speed. The study of the impact of enhanced wind speed and CLLJ in the lee of capes and headlands on the atmosphere has been studied (Nuss et al., 2000; Patricola and Chang, 2016). The direct impact of these enhanced wind speeds due to expansion fan processes in the local upwelling and SST, and on how locally generated waves interact with the upwelled cold waters remains to be studied. Also the interaction of the locally generated waves and the local wave driven currents, stronger in summer as shown by Carrasco et al. (2014) and the larger scale EBC is a subject that should be addressed in future research.

Climate change impact on the wind fields along the EBC systems has been the subject or recent research (Miranda et al., 2013; Semedo et al., 2016; Cardoso et al., 2016; Soares et al., 2016, 2017) It has been shown that coastal winds are projected to occur in the future, with West Iberia being on of the areas where potential changes might occur. In the context of wave climate projections studies (e.g. Hemer et al., 2013; Semedo et al., 2013; Dobrinyn et al., 2013, 2015), global to regional wave climate projections along the eastern boundary currents should therefore be studied.

Acknowledgements

Alvaro Semedo and Pedro M.M. Soares's work was done in the framework of the SOLAR project (PTDC/GEOMET/7078/2014), financed by the Portuguese Foundation for Science and Technology (FCT, Fundação para a Ciência e Tecnologia, in Portuguese). Gil Lemos is supported by FCT, through a doctoral grant PD/BD/135066/2017, within the Earth Systems Doctoral Program of the Faculty of Sciences of the University of Lisbon.

References

Aarnes, O.J., Abdalla, S., Bidlot, J.-R., Breivik, Ø., 2015. Marine wind and wave height trends at different ERA-Interim forecast ranges. J. Clim. 28, 819–837.
Alves, J.H., Banner, M.L., Young, I.R., 2003. Revisiting the Pierson-Moskowitz asymptotic limits for fully developed wind waves. J. Phys. Oceanogr. 33, 1301–1323.
Alves, J.H., 2006. Numerical modeling of ocean swell contributions to the global wind-wave climate. Ocean Model. 11 (1-2), 98–122.

Ardhuin, F., Jenkins, A., 2006. On the interaction of surface waves and upper ocean turbulence. J. Phys. Oceanogr. 33, 551–557.
Babanin, A.V., 2011. Breaking and Dissipation of Ocean Surface Waves. Cambridge Univ. Press, Cambridge, U. K., pp. 480. https://doi.org/10.1017/CBO9780511736162.
Babanin, A.V., Onorato, M., Qiao, F., 2012. Surface waves and wave-coupled effects in lower atmosphere and upper ocean. J. Geophys. Res. 117https://doi.org/10.1029/2012JC007932. *C00J01*.
Bakun, A., 1990. Global climate change and intensification of coastal ocean upwelling. Science 247, 198–201.
Beardsley, R.C., Dorman, C.E, Friehe, C.A, Rosenfield, L.K., Wyant, C.D., 1987. Local atmospheric forcing during the Coastal Ocean Dynamics Experiment 1: a description of the marine boundary layer and atmospheric conditions over a northern California upwelling region. J. Geophys. Res. 92, 1467–1488.
Bidlot, J-R, 2001. ECMWF Wave Model Products. ECMWF Newsletter, pp. 9–15 , No. 91, ECMWF, Reading, United Kingdom.
Burk, S.D., Thompson, W.T., 1996. The summertime low-level jet and marine boundary layer structure along the California coast. Mon. Weather Rev. 124, 668–686.
Cardoso, R.M., Soares, P.M.M., Lima, D.C.A., Semedo, A., 2016. The impact of climate change on the Iberian low-level wind jet: EUROCORDEX regional climate simulation. Tellus A 68, 29005. https://doi.org/10.3402/tellusa.v68.29005.
Caires, S., Sterl, A., 2005. 100-year return value estimates for ocean wind speed and significant wave height from the ERA-40 data. J. Clim. 18 (7), 1032–1048.
Carrasco, A., Semedo, A., Isachsen, P.E., Christensen, K.H., Saetra, Ø., 2014. Global surface wave drift climate from ERA-40: the contributions from wind-sea and swell. Ocean Dyn. 64 (12), 1815–1829.
Cavaleri, L., Bertotti, L., Lionello, P., 1991. Wind wave cast in the Mediterranean Sea. J. Geophys. Res. 98 (C8), 10739–10764.
Cavaleri, L., Fox-Kemper, B., Hemer, M., 2012. Wind waves in the coupled climate system. Bull. Am. Meteorol. Soc. 93, 1651–1661.
Chen, G., Chapron, B., Ezraty, R., Vandemark, D., 2002. A global view of swell and wind sea climate in the ocean by satellite altimeter and scatterometer. J. Atmos. Ocean Technol. 19, 1849–1859.
Dee, D.P., Uppala, S., 2009. Variational bias correction of satellite radiance data in the ERA-Interim reanalysis. Q. J. R. Meteor. Soc. 135, 1830–1841.
Dee, D.P., Uppala, S.M., Simmons, A.J., Berrisford, P., Poli, P., co-authors, 2011. The ERA-Interim reanalysis: configuration and performance of the data assimilation system. Q. J. R. Meteorol. Soc. 137, 553–597.
Dobrynin, M., Murawsky, J., Baehr, J., Ilyina, T., 2015. Detection and attribution of climate change signal in ocean wind waves. J. Clim. 28 (4), 1578–1591.
Drennan, W.M., Kahma, K.K., Donelan, M.A., 1999. On momentum flux and velocity spectra over waves. Bound.-Layer Meteor. 92, 489–515.
Gersbach, G.H., Pattiaratchi, C.B, Ivey, G.N., Cresswell, G.R., 1999. Upwelling on the south-west coast of Australia—source of the Capes Current. Cont. Shelf Res. Volume 19 (Issue 3), 363–400.
Gerling, T.W., 1992. Partitioning sequences and arrays of directional wave spectra into component wave systems. J. Atmos. Ocean. Technol. 9, 444–458.
Harris, D.L., 1966. The wave-driven wind. J. Atmos. Sci. 23, 688–693.
Hanley, K.E., Belcher, S.E., Sullivan, P.R., 2010. A global climatology of wind-wave interaction. J. Phys. Ocanogr. 40, 1263–1282.
Hanson, J.L., Phillips, O.M., 2001. Automated analysis of ocean surface directional wave spectra. J. Atmos. Ocean. Technol. 18, 277–293.
Hemer, M., Fan, Y., Mori, N., Semedo, A., Wang, X., 2013. Projected changes in wave climate from a multi-model ensemble. Nat. Clim. Change 3, 471–476. https://doi.org/10.1038/NCLIMATE1791.
Högström, U., Smedman, A.-S., Sahlée, E., Drennan, W.M., Kahma, K.K., Johansson, C., Pettersson, H., Zhang, F., 2009. The atmospheric boundary layer during swell - a field study of the governing mechanism. J. Atmos. Sci. 66, 2764–2779.
Högström, U., Smedman, A.-S., Semedo, A., Rutgersson, A., 2011. Comments on "A global climatology of windwave interaction. J. Phys. Oceanogr. 41, 1811–1813. https://doi.org/10.1175/JPO-D-10-05015.1.
Högström, U., Rutgersson, A., Sahlée, E., Smedman, A.-S., Hristov, T.S., Drennan, W.M., Kahma, K.K., 2013. Air–Sea interaction features in the Baltic Sea and at a Pacific trade-wind site: an inter-comparison study. Bound. Layer Meteorol. 147, 139–163. https://doi.org/10.1007/s10546-012-9776-8.
Holthuijse, L.H., 2008. Waves in Oceanic and Coastal Waters. pp. 387 Cambridge.
Hristov, T.S., Miller, S.D., Friehe, C.A., 2003. Dynamical coupling of wind and ocean waves through wave-induced air flow. Nature 422, 55–58. https://doi.org/10.1038/nature01382.
Janssen, PAEM, Doyle, J.D., Bidlot, J.-R., Hansen, B., Isaksen, L., Viterbo, P., 2002. Impact and feedback of ocean waves on the atmosphere. In: Perrie, W (Ed.), Advances in Fluid Mechanics - Atmos.-Ocean Interact. WIT press, Ashurst, pp. 155–197.
Janssen, P.A.E.M., 2004. The Interaction of Ocean Waves and Wind. Cambridge University Press, pp. 300.
Leitão, F., Baptista, V., Teodósio, M.A., Hughes, S.J., Vieira, V., Chicharo, L., 2014. The role of environmental and fisheries multi-controls in white seabream (Diplodus sargus) artisanal fisheries in Portuguese coast. Reg. Environ. Change. https://doi.org/10.1007/s10113-014-0726-5.
Lima, D.C.A., Soares, P.M.M., Cardoso, C.R., Semedo, A., 2018. A global view of coastal low-level wind jets using an ensemble of reanalyses. J. Clim. 31, 1525–1546. https://doi.org/10.1175/JCLI-D-17-0395.1.
Komen, G.J., Cavaleri, L., Donelan, M., Hasslemann, K., Hasslemann, S., Janssen, P.A.E.M., 1994. Dynamics and Modelling of Ocean Waves. Cambridge University Press, pp. 520.
Komen, G.J., Janssen, P.A.E.M., Makin, V., Oost, W., 1998. On the sea state dependence of the Charnock parameter. Glob. Atmos. Ocean. Syst. 5, 367–388.
McWilliams, J., Restrepo, J., 1999. The wave-driven ocean circulation. J. Phys. Oceanogr. 29, 2523–2540.
Miranda, P.M.A., Alves, J.M.R., Serra, N., 2013. Climate change and upwelling: response of Iberian upwelling to atmospheric forcing in a regional climate scenario. Clim. Dyn. 40, 2813–2824.
Munk, W.H., Miller, G.R., Snodgrass, F.E., Barber, N.F., 1963. Directional recording of swell from distant storms. Philos. Trans. R. Soc. A255, 505–584 London.
Narayan, N., Paul, A., Mulitza, S., Schulz, M., 2010. Trends in Coastal Upwelling Intensity. Ocean Sci. 6, 815–823.
Nuss, W.A., Bane, J.M, Thompson, W.T., Holt, T., Dorman, C.E., Ralph, F.M., Rotunno, R., Klemp, J.B., Skamarock, W.C., Rogerson, A.M., Reason, C., Jackson, P., 2000. Coastally trapped wind reversals: a new level of understanding from the experiment on coastally trapped disturbances. Bull. Am. Meteorol. Soc. 81, 719–743.
Pandian, P.K., Emmanuel, O., Ruscoe, J.P., Side, J.C., Harris, R.E., Kerr, S.A., Bullen, C.R., 2011. An overview of recent technologies on wave and current measurement in coastal and marine applications. J. Oceanogr. Mar. Sci. 1 (1), 001–010.
Pastor, M.V., Vélez-Belchí, P., Hernández-Guerra, A., 2015. Water masses in the canary current large marine ecosystem. In: Valdés, L., Déniz-González, I. (Eds.), Oceanographic and Biological Features in the Canary Current Large Marine Ecosystem. IOC-UNESCO, Paris, pp. 73–79 IOC Technical Series.
Patricola, C., Chang, P., 2016. Structure and dynamics of the Benguela low-level coastal jet. Clim. Dyn. https://doi.org/10.1007/s00382-016-3479-7.
Pierson, W.J., Moskowitz, L., 1964. A proposed spectral form for fully developed wind seas based on the similarity theory of S.A. Kitaigorodskii. J. Geophys. Res. 69, 5181–5190.
Potter, H., 2015. Swell and the drag coefficient. Ocean Dyn. 65 (3), 375–384.
Ranjha, R., Svensson, G., Tjernström, M., Semedo, A., 2013. Global distribution and seasonal variability of coastal low-level jets derived from ERA-Interim reanalysis. Tellus A 65, 20412. http://dx.doi.org/10.3402/tellusa.v65i0.20412.
Ranjha, R, Tjernström, M., Semedo, A., Svensson, G., Cardoso, R.M., 2015a. Structure and variability of the oman coastal low-level jet. Tellus A 67, 25285. http://dx.doi.org/10.3402/tellusa.v67.25285.
Ranjha, R, Tjernström, M., Svensson, G., Semedo, A., 2015b. Modeling coastal low-level wind-jets: does horizontal resolution matter. Met. Atmos. Phys. 128, 263–278. https://doi.org/10.1007/s00703-015-0413-1.
Rutgerson, A., Saetra, Ø., Semedo, A., Carlson, B., Kumar, R., 2010. Impact of surface waves in a Regional Climate Model. Meteorol. Az. 19 (3), 247–257.
Rijo, N., Lima, D.C.A., Semedo, A., Miranda, P.M.A., Cardoso, R., 2014. The Iberian Peninsula lowlevel coastal jet: climatology and case study analysis. In: Proceedings 10th Jornadas do Mar, November. Lisbon. pp. 11–14 2014.
Rijo, N., Semedo, A., Lima, D.C.A., Miranda, P.M.A., Cardoso, R., Soares, P.M.M., 2015. The northerly summer wind off the west coast of the Iberian Peninsula. In: Proceedings of TransNav 2015 - International Conference on "Marine Navigation and Safety of Sea Transportation. Gdynia, Poland. 17-19 June 2015.
Rijo, N., Semedo, A., Miranda, P.M.A., Lima, D.C.A., Cardoso, R.M., Soares, P.M.M., 2017. Spatial and temporal variability of the Iberian Peninsula coastal low-level jet. Int. J. Climatol. 38 (4), 1605–1622. https://doi.org/10.1002/joc.5303.
Semedo, A., Sušelj, K., Rutgersson, A., 2008. Variability of Wind sea and swell waves in the north atlantic based on ERA-40 reanalysis. In: Proceedings of the 8th European Wave and Tidal Energy Conference. Uppsala, Sweden. September 7-10, 2008.
Semedo, A, Sætra, Ø., Rutgersson, A., Kahma, K.K., Pettersson, H., 2009. Wave induced wind in the marine boundary layer. J. Atmos. Sci. 66, 2256–2271.
Semedo, A, 2010. Atmosphere–ocean interactions in swell dominated wave fields. Ph.D. thesis. Uppsala University, Sweden.
Semedo, A, Sušelj, K., Rutgersson, A., Sterl, A., 2011. A global view on the wind sea and swell climate and variability from ERA-40. J. Clim. 24 (5), 1461–1479.
Semedo, A., Rutgersson, A., Sterl, A., Sušelj, K., et al., 2012. The global wave age climate. In: Soares (Ed.), Marine Engineering and Technology. Taylor and Francis Group, London, pp. 539–543.
Semedo, A., Weisse, R., Beherens, A., Sterl, A., Bengtsson, L., Gunther, H., 2013. Projection of global wave climate change towards the end of the 21st century. J. Clim. 26, 8269–8288.
Semedo, A., Vettor, R., Breivik, Ø., Sterl, A., Reistad, M., Soares, C.G., Lima, D., 2015. The wind sea and swell waves climate in the Nordic seas. Ocean Dyn. 65, 223–240. https://doi.org/10.1007/s10236-014-0788-4.
Small, C., Nicholls, R.J., 2003. A global analysis of human settlement in coastal zones. J. Coast. Res. 19, 584–599.
Smedman, A.-S., Högström, U., Bergström, H., Rutgersson, A., Kahma, K.K., Pettersson, H., 1999. A case-study of air-sea interaction during swell conditions. J. Geophys. Res. 104 (25) , 833-25,851.
Smedman, A.-S., Högström, U., Sahleé, E., Drennan, W.M., Kahama, K.K., Pettersson, H., Zhang, F., 2009. Observational study of marine atmospheric boundary layer characteristics during swell. J. Atmos. Sci. 66, 2747–2763.
Snodgrass, F.E., Groves, G.W., Hasselmann, K.F., Miller, G.R., Munk, W.H., Powers, W.M., 1966. Propagation of swell across the Pacific. Philos. Trans. R. Soc. A259, 431–497 London.
Soares, P.M.M., Cardoso, R., Semedo, A., Chinita, M.J., Ranjha, R., 2014. The Iberian Peninsula coastal low level jet. Tellus A 66, 22377. https://doi.org/10.3402/tellusa.v66.22377.
Soares, P.M.M., Lima, D.C.A., Cardoso, R.M., Semedo, A., 2016. High resolution projections for the Western Iberian Coastal Low level jet in a changing climate. Clim. Dyn. http://dx.doi.org/10.1007/s00382-016-3397-8.
Soares, P.M.M., Lima, D.C.A., Cardoso, R.M., Nascimento, M.L., Semedo, A., 2017. Western Iberian offshore wind resources: more or less in a global warming climate? Appl. Energy 203, 72–90.
Sterl, A., 2004. On the (in-)homogeneity of reanalysis products. J. Clim. 17, 3866–3873.
Sterl, A., Caires, S., 2005. Climatology, variability and extrema of ocean waves: The Web-

based KNMI/ERA-40 wave atlas. Int. J. Climatol. 25, 963–997. https://doi.org/10.1002/joc.1175.
Stopa, J., Cheung, K.F., 2014. Intercomparison of wind and wave data from the ECMWF reanalysis Interim and the NCEP Climate Forecast System Reanalysis. OC Model. 75, 65–83.
Stopa, J., Ardhuin, F., Girard-Ardhuin, F., 2016. Wave climate in the Arctic 1992–2014: seasonality and trends. Cryosphere 10, 1605–1629.
Sullivan, P.P., Edson, J.B., Hristov, T., McWilliams, J.C., 2008. Large-eddy Simulations and observations of atmospheric marine boundary layers above nonequilibrium surface waves. J. Atmos. Sci. 65, 1225–1254.
Tuomi, L, Kahma, K.K., Pettersson, K., 2011. Wave hindcast statistics in the seasonally ice covered baltic sea. Boreal Environ. Res. 16, 451–472.
Tjernström, M., Grisogono, B., 2000. Simulations of supercritical flow around points and capes in the coastal atmosphere. J. Atmos. Sci. 57, 108135.
Uppala, S.M., 1997. ECMWF Re-Analysis Project Report Series 3. ECMWF, pp. 261.
Uppala, S.M., Coauthors, 2005. The ERA-40 re-analysis. Q. J. R. Meteorol. Soc. 131, 2961–3012 Ursel, F., 1956: Surveys in mechanics.
Ursel, F., 1956. Surveys in Mechanics. In: Batchelor, G.K. (Ed.), pp. 216–249 London-Cambridge.
Vallis, G.K., 2000. Large-scale circulation and production of stratification: efects of wind, geometry and difusion. . J. Phys. Oceanogr. 30, 933–954.
Violante-Carvalho, N., Robinson, I.S., Schulz-Stellenfleth, J., 2005. Assessment of ERS synthetic aperture radar wave spectra retrieved from the Max-Planck-Institut (MPI) scheme through inter-comparisons of 1 year of directional buoy measurements. J. Geophys. Res. 110, C07019. https://doi.org/10.1029/2004JC002382.
Young, I.R., 1999. Seasonal variability of the global ocean wind and wave climate. Int. J. Climatol. 19, 931–950.
WAMDI Group, 1988. TheWAMmodel—a third generation oceanwave prediction model. J. Phys. Oceanogr. 18 1775–181.
Winant, C.D., Dorman, C.E., Friehe, C.A, Beardsley, R.C., 1988. The marine layer off Northern California: an example of supercritical channel flow. J. Atmos. Sci. 45, 3588–3605.